Utah State University

DigitalCommons@USU

All Graduate Theses and Dissertations | Graduate Studies

12-2022

Bifurcations and Hysteresis in the Dynamics of Small Populations of Spherical Magnets

Peter T. Haugen
Utah State University

Follow this and additional works at: https://digitalcommons.usu.edu/etd

 Part of the Physics Commons

Recommended Citation

Haugen, Peter T., "Bifurcations and Hysteresis in the Dynamics of Small Populations of Spherical Magnets" (2022). *All Graduate Theses and Dissertations*. 8625.
https://digitalcommons.usu.edu/etd/8625

This Dissertation is brought to you for free and open access by the Graduate Studies at DigitalCommons@USU. It has been accepted for inclusion in All Graduate Theses and Dissertations by an authorized administrator of DigitalCommons@USU. For more information, please contact digitalcommons@usu.edu.

UtahStateUniversity
MERRILL-CAZIER LIBRARY

BIFURCATIONS AND HYSTERESIS IN THE DYNAMICS OF SMALL POPULATIONS OF SPHERICAL MAGNETS

by

Peter T. Haugen

A dissertation submitted in partial fulfillment
of the requirements for the degree

of

DOCTOR OF PHILOSOPHY

in

Physics

Approved:

Boyd F. Edwards, Ph.D. Major Professor	Charles Torre, Ph.D. Committee Member
Jim Wheeler, Ph.D. Committee Member	Eric Held, Ph.D. Committee Member
David Farrelly, Ph.D. Committee Member	D. Richard Cutler, Ph.D. Vice Provost of Graduate Studies

UTAH STATE UNIVERSITY
Logan, Utah

2022

Copyright © Peter T. Haugen 2022

All Rights Reserved

ABSTRACT

Bifurcations and Hysteresis in the Dynamics of Small Populations of Spherical Magnets

by

Peter T. Haugen, Doctor of Philosophy

Utah State University, 2022

Major Professor: Boyd F. Edwards, Ph.D.
Department: Physics

Spherical permanent magnets present an appealing opportunity to study the dynamics of bodies with dipole interactions due to their ubiquity and exceptionally close approximation to ideal dipoles. Starting with the interaction potential between two dipoles we investigate the dynamics of two identically magnetized spheres sliding against each other and show that their motion at all scales while they remain in contact is isomorphic with two uncoupled pendulums after a coordinate transform. One of the system's modes can have an arbitrary amount of energy imparted and the spheres maintain contact, while the other mode possesses a cut off point where the two spheres break contact and new dynamics take hold.

The same interaction potential is then used to examine a system of six identical dipoles fixed at the vertices of a regular hexagon with a seventh dipole of variable dipole strength in the center. Their dipole moments are free to spin while constrained to orient entirely in the plane of the hexagon and these orientations are examined. Macroscopic static properties including net dipole moment and total potential energy are calculated and compared with observation in two cases. Its normal modes of oscillation are also calculated and compared with analytic results in two cases. Two distinct states of all these phenomena are observed with discontinuous bifurcations as well as hysteresis.

(58 pages)

PUBLIC ABSTRACT

Bifurcations and Hysteresis in the Dynamics of Small Populations of Spherical Magnets

Peter T. Haugen

If you heat up some kinds of metals and then cool them down next to a magnet, they will be a magnet when they cool, but if they cool down away from a magnet, they will just be a lump of metal. This is an example of hysteresis and it's very important for lots of technology. Another example of hysteresis might be a water tower pump that turns on when the tower is nearly empty and keeps going until the tower is nearly full. Whether or not the pump is on when the tower is half full depends on what the condition of the tower was recently. Hysteresis more generally can be thought of as when somethings present condition depends very strongly on what it's history was. A counter example would be for a gas, when you know it's temperature and pressure and volume, that's all that matters.

Many systems with hysteresis are complicated, but this research has found that some very simple arrangements of the simplest magnets can have still have hysteresis. I show this primarily by looking at how the systems move around their resting position.

This research was funded by an NSF grant.

To:
My patient and accommodating advisor Dr. Edwards.
My supportive and nurturing parents, Alice and Tom.
All my many other exasperated teachers and mentors.
And most importantly to my dearest Amy.

ACKNOWLEDGMENTS

To coffee, without which many graduate students' work would go unfinished.

And to antidepressants, without which many graduate students' work would be finished tragically early.

Peter Haugen

CONTENTS

Page

ABSTRACT . . . iii

PUBLIC ABSTRACT . . . v

ACKNOWLEDGMENTS . . . vii

LIST OF TABLES . . . x

LIST OF FIGURES . . . xi

1 Introduction . . . 1
- 1.1 Background . . . 1
- 1.2 Methods . . . 2
  - 1.2.1 Potential Energy . . . 2
  - 1.2.2 Kinetic Energy . . . 3
  - 1.2.3 Equations of Motion . . . 4
  - 1.2.4 Equilibrium and Linearization . . . 4
  - 1.2.5 Higher Dimensions . . . 5

2 Dynamics of Two Freely Rotating Dipoles . . . 7
- 2.1 Introduction . . . 7
- 2.2 Describing the System . . . 8
  - 2.2.1 Coordinates . . . 8
  - 2.2.2 Hamiltonian . . . 9
  - 2.2.3 Dimensionless coordinates . . . 10
- 2.3 Analysis . . . 11
  - 2.3.1 Analytic Results . . . 11
  - 2.3.2 Numerical Results . . . 17
- 2.4 Conclusions . . . 19

3 Hysteresis in A System of Seven Magnets . . . 20
- 3.1 Introduction . . . 20
- 3.2 System And Methods . . . 21
  - 3.2.1 Geometry . . . 21
  - 3.2.2 Equations of Motion . . . 22
- 3.3 Analysis . . . 24
  - 3.3.1 Comparing with Prior Results . . . 24
  - 3.3.2 Normal Modes of Oscillation . . . 26
  - 3.3.3 Large α Limit . . . 29
- 3.4 Conclusions . . . 34

4 Base Case for Magnet Systems Exhibiting Hysteresis 35
4.1 Introduction 35
4.2 Why Two Dipoles Are Unremarkable 35
4.3 Three Dipoles in a Line 36
4.4 The Triangular Case 37

5 Conclusions 42

REFERENCES 43

Curriculum Vitae 45

LIST OF TABLES

Table Page

4.1 A summary of the eigenfrequencies and how they vary with α in the two cases for a set of three linearly arranged dipoles. 37

LIST OF FIGURES

Figure Page

1.1 In this figure **m** is used to denote dipole moment. 3

2.1 Schematic of labeling system describing two spheres in the plane featuring both the independent coordinates and the center of mass coordinates. . . . 8

2.2 Numerical results for four frames of an orbital mode with period 3 (top row), and a spinning mode with period 8 (bottom row). 14

2.3 Above is a plot of large amplitude period vs. total system energy. 18

3.1 Diagram depicting six dipoles arranged at the vertices of a regular hexagon with a seventh dipole at the center. 21

3.2 Schematic representations of the seven eigenmodes of oscillation about the circular state for a central dipole with relative strength $\alpha = 1.3$. 25

3.3 Panel (a) is the eigenvalue ω^2 vs. α for each of the seven modes of oscillation about the circular state, labeled based on ascending order at $\alpha = 0$. 27

3.4 Panels (a) through (d) are the vectors corresponding to modes 4 through 7 about the circular state. 28

3.5 R_i is the ratio of eigenvalue ω_i^2/α at α and its projected value for $\alpha \to \infty$. 31

3.6 Panel (a) is $\omega^2\alpha^{-1}$ vs. α^{-1} while panels (b) through (d) depict the vectors corresponding to the perturbations of the first three modes in the dipole state presented in the same fashion as Fig. 3.3. 32

3.7 Panel (a) through (d) are the perturbations of the remaining four modes in the dipole state presented in the same fashion as Fig. 3.3. 33

4.1 Dipoles arranged in an equilateral triangle. 37

4.2 The normal mode information for the low α state. 39

4.3 The normal mode information for the high α state. 40

4.4 The potential energy of the ground state as a function of α. 41

CHAPTER 1

Introduction

1.1 Background

The monopole term is dominant in systems governed by gravity because negative mass has yet to make its way off the chalkboard and into observation, let alone be present in equal amounts as normal mass. Meanwhile, the dipole term has far more longevity and importance in the realm of electromagnetism. The dipole moment of a water molecule is responsible for many of its bizarre and helpful properties. The dipole term is the strongest term yet observed for magnetic objects and has been exploited for navigational purposes for over two millennia. Simple permanent magnets have been employed in making electricity with generators for over a century. Now permanent magnets are being used in mechanical contexts, such as gears, latches and motors with a variety of advantages including smoothness of force transmission, longevity and failing gracefully under excessive loads [1].

Systems with statistically large numbers of dipoles already are a rich field of study as they are the basis of the Ising model and are one of the preferred models featuring group phenomena such as phase transitions. Slightly less well studied are small quantities of dipoles. These smaller sets correspond more closely to the burgeoning field of magnetomechanical engineering and more basic analyses of their building blocks may provide useful insights.

Some systems with small numbers of dipoles have been explored previously. Pollack examined the rotation of two dipoles that are free to spin about fixed axes [2]. Stump et al. investigated the normal modes for arbitrary numbers of dipoles that are fixed at the vertices of a regular polygon [3]. Edwards et al. showed that a uniformly magnetized sphere generates and interacts with magnetic fields as though it were a point dipole [4], setting a context for the examination of a dipole that slides freely along the surface of another fixed dipole [5] and the dynamics of a free dipole bouncing against a fixed dipole [6, 7].

1.2 Methods

Approaching the dynamics of magnetic dipoles from the direction of Newton's equations of motion would entail determining the torques applied to each dipole and determining angular accelerations from there. There is some discourse [8–11] as to how to calculate those torques, so to obviate that question entirely I skipped straight to Lagrange's equations of motion. This had the added benefit that the results found were more adaptable. This adaptability makes the method generally more appealing as a matter of personal taste. To find the Lagrange equations of motions for a system we need to describe its potential energy and its kinetic energy.

1.2.1 Potential Energy

The interaction potential [12] that captures the behavior at time scales slow enough to disregard radiation is

$$U = \frac{\mu_0}{4\pi}\frac{1}{r^3}\left[\mathbf{m}_1 \cdot \mathbf{m}_2 - 3(\mathbf{m}_1 \cdot \mathbf{r})(\mathbf{m}_2 \cdot \mathbf{r})r^{-2}\right], \tag{1.1}$$

where $\mathbf{m}$ is a magnetic dipole as a vector, $\mathbf{r}$ and r are the separation vector and absolute distance between the two dipoles, and μ_0 is the magnetic permeability of the vacuum. The geometry is shown pictorially in figure 1.1. In the case where all three vectors are co-planar the expression can be simplified down to [5]

$$U = -\frac{\mu_0}{4\pi}\frac{m_1 m_2}{2r^3}[\cos(\phi_1 - \phi_2) + 3\cos(\phi_1 + \phi_2 - 2\theta)], \tag{1.2}$$

where the angles ϕ_1, ϕ_2 and θ reference the angle between some vector and a common axis. The angles ϕ_1 and ϕ_2 relate to the orientation of dipoles one and two respectively, while θ describes the orientation of the separation vector $\mathbf{r}$.

where ϕ_1 and ϕ_2 represents the angle that that dipole's orientation makes with some specified axis and θ represents the angle the separation vector $\mathbf{r}$ makes with the previously mentioned axis. For the sake of concreteness I'll be referencing those angles as deflections

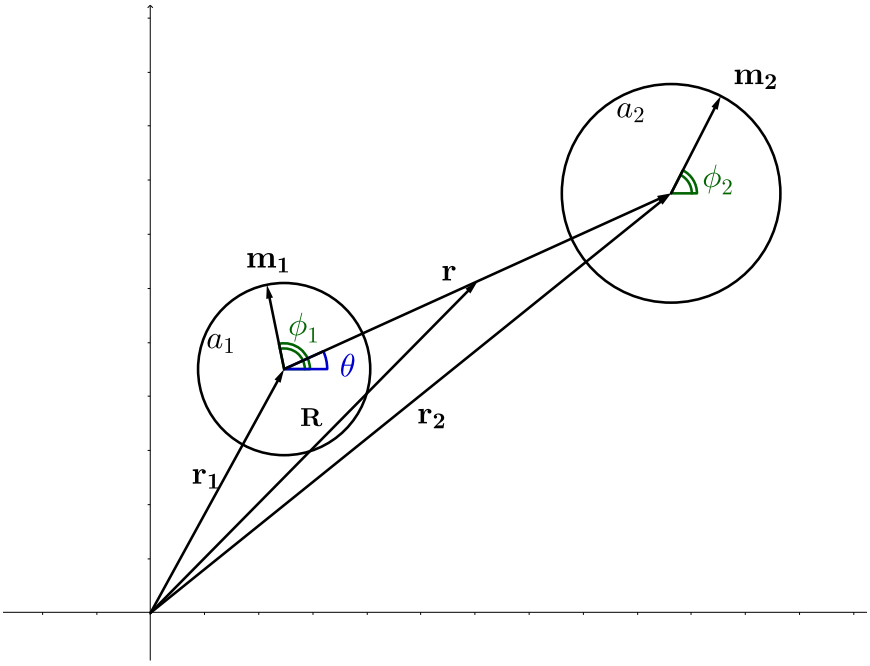

Figure 1.1: In this figure **m** is used to denote dipole moment.

from the x-axis.

1.2.2 Kinetic Energy

The kinetic energy of a sphere is

$$T_i = \frac{1}{2}(M_i \dot{\mathbf{r}}^2 + I_i \dot{\phi}_i^2), \tag{1.3}$$

where $\dot{\mathbf{r}}$ refers to the change in the sphere's position over time and governs the translational component of the sphere's kinetic energy, while $\dot{\phi}$ refers to its rotation around an axis over time and governs the rotational component of the kinetic energy. Because we are limiting our investigations to spheres, the moment of inertia I is a constant, rather than a tensor as would be the fully general case, and the angular velocity likewise is a scalar. In the case where the sphere is fixed in space, or we have chosen an inertial frame of reference where the sphere is stationary, the translational component would be fixed at zero.

1.2.3 Equations of Motion

Equipped with expressions for potential and kinetic energies, Lagrange's equations of motion are determinable. The quantity

$$\mathcal{L} = T - U \tag{1.4}$$

is known as the Lagrangian and when a system's kinetic and potential energy functions are used it can provide the equations of motion for that system as

$$\partial_q \mathcal{L} = \frac{d}{dt}(\partial_{\dot{q}} \mathcal{L}), \tag{1.5}$$

where ∂_q is an operator taking the partial derivative with respect to some general coordinate q of the quantity it's acting on. The fact that q is entirely arbitrary is the major strength of this method. It could be a position relative to some axis like cartesian coordinates, or it could be a relative position to some other object, a displacement along some prescribed curve, an orientation, or even some strange combination of all the above.

1.2.4 Equilibrium and Linearization

While these equations can be generated for wide range of interaction potentials they are rarely solvable, in the sense of determining closed form solutions for the evolution of a state in time. Frequently even determining equilibrium states where all the net forces are zero requires resorting to numerical methods. But supposing you know the equilibrium of a system, you can learn something about the system's dynamics.

First in the one dimensional case where $\partial_q \mathcal{L} = -\partial_q U$ and the potential is lacking any pathologies like discontinuities at the equilibrium it is possible to approximate the potential near a point q_0 as

$$U(q) \approx U|_{q_0} + \partial_q U|_{q_0}(q - q_0) + \partial_q^2 U|_{q_0} \frac{(q_0 - q)^2}{2} + \mathcal{O}((q_0 - q)^3) \tag{1.6}$$

This leaves the domain of mathematical curiosity and becomes incredibly useful when q_0

is an equilibrium of Eq. 1.5. If that is the case, $\partial_q U|_{q_0} = 0$ by the nature of equilibrium. And since $U|_{q_0}$ does not vary in q it is irrelevant when we try to determine equations of motion by taking derivatives. While $|q_0 - q| << 1$, we can ignore the higher order terms and are left with a harmonic potential and its attendant natural frequency. This approximation is only valid for small deviations from equilibrium, arising either from initial conditions or a stochastic external force. However it highlights stimuli that could excite large deviations from equilibrium as periodic forcing at the natural frequency would cause a resonant response, typically causing motion where $|q_0 - q| << 1$ was no longer true. This is useful knowledge for experimental design as it might be the first step to observing interesting phenomena.

1.2.5 Higher Dimensions

If there are two or more degrees of freedom in the system the natural frequency analysis can still be done straightforwardly in the case where $\partial_{\dot{q}_i}\mathcal{L}$ is linear in $\dot{q}_i$, or, symbolically, expressible as $M_i\dot{q}_i$ where M_i is a constant. This condition and knowing an equilibrium state $\mathbf{q}^*$ allows us to write out an approximation of the equations of motion as

$$M_i\ddot{q}_i \approx -\partial_{q_i}\Sigma_j\Sigma_k \left[\left(\partial_{q_j}\partial_{q_k}U\right)|_{\mathbf{q}^*}\right](q_j - q_j^*)(q_k - q_k^*) = \Sigma_j \left[\left(-\partial_{q_j}\partial_{q_i}U\right)|_{\mathbf{q}^*}\right](q_j - q_j^*) \quad (1.7)$$

where i, j and k are indices for the degrees of freedom. This approximation of the equations of motion already produces periodic motion, so we may assume solutions of the form

$$\mathbf{q}(t) = \mathbf{q}^* + \delta\mathbf{q}(t), \quad (1.8)$$

where

$$\delta\mathbf{q}(t) = \mathbf{a}\exp(i\omega t). \quad (1.9)$$

This allows us to rewrite the left hand of equation 1.7 as

$$\ddot{q}_i = \ddot{\delta q}_i = -\omega^2 a_i \exp(-i\omega t). \quad (1.10)$$

If we define matrices $\widehat{M}$ and $\widehat{K}$ as

$$M_{i,i} = M_i, \tag{1.11}$$

and

$$K_{i,j} = \partial_{q_i}\partial_{q_j}U. \tag{1.12}$$

Then we can rewrite the whole set of equations as the matrix problem

$$-\omega^2\widehat{M}\delta\mathbf{q}(t) = -\widehat{K}\delta\mathbf{q}(t) \tag{1.13}$$

or

$$\left(\widehat{K} - \omega^2\widehat{M}\right)\delta\mathbf{q}(t) = 0. \tag{1.14}$$

For the non-trivial case where there is any movement at all, equation 1.14 will only hold if $\mathbf{a}$ is an eigenvector and ω^2 is an eigenvalue of $\widehat{K} - \omega^2\widehat{M} = \widehat{P}$ which I will refer to as the perturbation matrix from this point. The vector $\mathbf{a}$ was the directional component of the periodic assumption that was made in equation 1.9. For a system with N degrees of freedom, there will be up to N pairs of eigenvalues and eigenvectors, or taken together, normal modes. If all the eigenvalues are unique, then the eigenvectors are fully determined and have the property of all being mutually orthogonal. They can also be combined to describe any initial condition in the space, a property known as being a spanning set. If some of the eigenvalues are identical, also known as degenerate, then there is some indeterminacy and the eigenvectors associated with the degenerate eigenvalues can take any value so long as the set as a whole remains mutually orthogonal and spanning.

CHAPTER 2

Dynamics of Two Freely Rotating Dipoles

2.1 Introduction

To begin, we'll examine the simplest number of magnets possible, two dipoles interacting absent any additional fields. In looking at a pair of unrestrained magnetized spheres we've taken a simpler system and increased its degrees of freedom. While it's common to maintain the same level of complexity of the motion or increase it, here we find that making the phase space more complex decreases the complexity of the motion.

Several simple cases have been examined analytically. Pollack [2] has investigated interactions between two point dipoles fixed in space but which are free to rotate, and finds quasi periodic motion. Edwards et al. has taken advantage of some work that shows magnetized spheres experience magnetic fields as though those spheres were point dipoles [4] to discover how one sphere freely sliding around on the surface of another sphere that is fixed in space and orientation leads to chaotic motion [5]. Fixing one sphere breaks the symmetry in space equivalent to an external torque and prevents conserved total angular momentum from arising.

We take a union of the Pollack and Edwards systems by allowing both spheres to freely rotate and slide along each other. While each of these systems has two degrees of freedom, they are different pairs chosen from the more general case and thus not immediately comparable. Our combined system has three degrees of freedom. While Edwards' system exhibited chaos, this new system does not, even at large amplitudes. It is shown to exhibit separate pieces of movement with irrational frequencies, resulting in quasi-periodic behavior, rather than chaos.

Numerical methods have been developed for arbitrarily complicated arrangements [13] and by examining this simple case analytically we can provide an additional check on their

results.

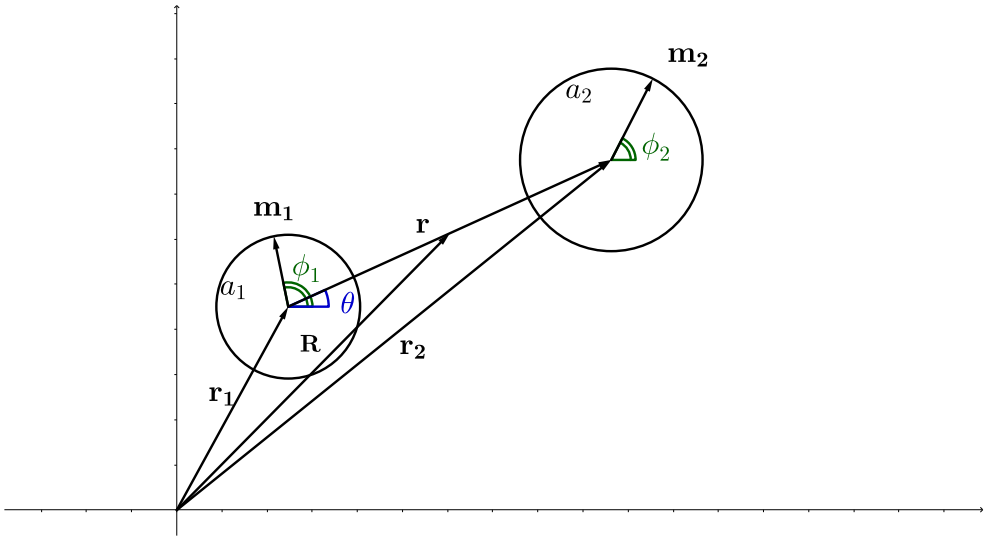

Figure 2.1: Schematic of labeling system describing two spheres in the plane featuring both the independent coordinates and the center of mass coordinates.

2.2 Describing the System

Intrinsic properties of the two dipoles are: their respective radii, which we shall label as a_1 and a_2, their masses, M_1 and M_2, and magnitudes of their dipole moments, m_1 and m_2.

2.2.1 Coordinates

Cartesian

Each of the dipoles has a location constrained to the x-y plane $\mathbf{r_1}$ and $\mathbf{r}_2$ along with an orientation for the dipole ϕ_1 and ϕ_2 which we will also constrain to the x-y plane, measured from the x-axis.

Center Of Mass

We can define a set of composite coordinates and quantities more appropriate for

analyzing two-body system using the aforementioned independent coordinates following Taylor's approach [14].

These composite coordinates are as follows: the total and reduced mass,

$$M_t = M_1 + M_2, \qquad M_r = \frac{M_1 M_2}{M_1 + M_2}, \tag{2.1}$$

the center of mass,

$$\mathbf{R} = \frac{M_1 \mathbf{r}_1 + M_2 \mathbf{r}_2}{M_t}, \tag{2.2}$$

and the displacement of dipole 2 from dipole 1,

$$\mathbf{r} = \mathbf{r}_2 - \mathbf{r}_1 = \mathrm{r}[\cos(\theta)\hat{\mathbf{x}} + \sin(\theta)\hat{\mathbf{y}}]. \tag{2.3}$$

Here θ is the angle $\mathbf{r}$ makes with the x-axis.

2.2.2 Hamiltonian

To take advantage of the numerous analytic techniques that can be applied to a system's Hamiltonian, it must first be calculated. This in turn requires that we find its kinetic and potential energy in terms of its coordinates.

Energies

The kinetic energy, T, is [14]

$$\begin{aligned} T &= \frac{1}{2}(M_1 \dot{\mathbf{r}_1}^2 + M_2 \dot{\mathbf{r}_2}^2 + I_1 \dot{\phi_1}^2 + I_2 \dot{\phi_2}^2) \\ &= \frac{1}{2}(M_t \dot{R}^2 + M_r \dot{r}^2 + M_r r^2 \dot{\theta}^2 + I_1 \dot{\phi_1}^2 + I_2 \dot{\phi_2}^2). \end{aligned} \tag{2.4}$$

The first three terms in the second equation are for two bodies in center of mass coordinates with the final two terms accounting for the internal degrees of freedom of the spheres. The potential interaction between two dipoles was addressed in the introduction in equation 1.2.

Having an expression for kinetic and potential energy, the Lagrangian is

$$\begin{aligned} L = T - U = \frac{1}{2}(M_t\dot{R}^2 + M_r\dot{r}^2 + M_r r^2\dot{\theta}^2 + I_1\dot{\phi}_1^2 + I_2\dot{\phi}_2^2) \\ + \frac{\mu_0}{4\pi}\frac{m_1 m_2}{2}\frac{1}{r^3}[\cos(\phi_1 - \phi_2) + 3\cos(\phi_1 + \phi_2 - 2\theta)]. \end{aligned} \tag{2.5}$$

It might be noted that this Lagrangian takes into account only magnetostatic interactions which ignores the resulting damping one would see from accelerating dipoles which would necessarily happen anytime the system is away from equilibrium. The scale of those corrections will be addressed in a later section.

Momenta

The first observation we make is that the Lagrangian is independent of the center of mass position making the corresponding momenta a constant of motion and we will proceed assuming we are in the inertial frame where the center of mass momentum is 0 and R is 0. Determining the other momenta we use the relationship $\partial_{\dot{q}_i} L = p_i$ to arrive at

$$\partial_{\dot{\phi}_1} L = I_1\dot{\phi}_1 = p_{\phi_1}, \tag{2.6a}$$

$$\partial_{\dot{\phi}_2} L = I_2\dot{\phi}_2 = p_{\phi_2}, \tag{2.6b}$$

$$\partial_{\dot{\theta}} L = M_r r^2\dot{\theta} = p_\theta, \tag{2.6c}$$

$$\partial_{\dot{r}} L = M_r\dot{r} = p_r. \tag{2.6d}$$

Allowing us to find the Hamiltonian with the expression of

$$H = \Sigma_i p_i\dot{q}_i - L = \frac{1}{2}\left(\frac{p_r^2}{M_r} + \frac{p_\theta^2}{M_r r^2} + \frac{p_{\phi_1}^2}{I_1} + \frac{p_{\phi_2}^2}{I_2}\right) + U(\phi_1, \phi_2, \theta, r). \tag{2.7}$$

2.2.3 Dimensionless coordinates

To get at the essentials of the system we will examine it in a natural set of dimensions. First we will characterize the second dipole in terms of the first such that $M_2 = \alpha M_1$,

$a_2 = \beta a_1$, $m_2 = \gamma m_1$. This lets us rewrite the energies as

$$T = \frac{1}{2}\left[\frac{(1+\alpha)M_1}{\alpha M_1^2}p_r^2 + \frac{(1+\alpha)M_1}{\alpha M_1^2}\frac{p_\theta^2}{r^2} + p_{\phi_1}^2\frac{5}{2M_1a_1^2} + p_{\phi_2}^2\frac{1}{\alpha\beta^2}\frac{5}{2M_1a_1^2}\right], \tag{2.8a}$$

$$U = -\frac{\mu_0}{4\pi}\frac{\gamma m_1^2}{2}\frac{1}{r^3}[\cos(\phi_1-\phi_2) + 3\cos(\phi_1+\phi_2-2\theta)]. \tag{2.8b}$$

We go on to define our units as follows: $L_0 = 2a_1$ for length, m_1 for magnetic moment, $F_0 = 3\mu_0 m_1^2/(2\pi L_0^4)$ for force, F_0L_0 for energy, $T_0 = \sqrt{M_1L_0/F_0}$ for time, T_0^{-1}, T_0^{-2} for angular velocities and accelerations, M_1L_0/T_0 for linear momentum and $M_1L_0^2/T_0$ for angular momentum. This lets us rewrite the energies as

$$T = \frac{1}{2}\left[\frac{(1+\alpha)}{\alpha}p_r^2 + \frac{(1+\alpha)}{\alpha}\frac{p_\theta^2}{r^2} + 10p_{\phi_1}^2 + \frac{10}{\alpha\beta^2}p_{\phi_2}^2\right], \tag{2.9a}$$

$$U = -\frac{\gamma}{12}\frac{1}{r^3}[\cos(\phi_1-\phi_2) + 3\cos(\phi_1+\phi_2-2\theta)]. \tag{2.9b}$$

Let us finally make two more assumptions. First, that the two spheres are identical, $\alpha = \beta = \gamma = 1$. Second, that there is some contact potential energy U_C preventing the two spheres from overlapping that prohibits r from getting less than 1. These two assumptions produce the Hamiltonian we'll be investigating for the remainder of our discussion

$$\begin{aligned} H = T + U = \frac{1}{2}\left(2p_r^2 + 2\frac{p_\theta^2}{r^2} + 10p_{\phi_1}^2 + 10p_{\phi_2}^2\right) \\ - \frac{1}{12}\frac{1}{r^3}[\cos(\phi_1-\phi_2) + 3\cos(\phi_1+\phi_2-2\theta)] + U_C. \end{aligned} \tag{2.10}$$

2.3 Analysis

2.3.1 Analytic Results

Equilibrium Analysis

Let us first examine the equations of motion and see if there exist any equilibria between the spheres while they are in contact with each other ($r = 1$). The Hamiltonian equations

of motion we find are

$$\dot{p}_{\phi_1} = -\partial_{\phi_1} H = -\frac{1}{12}\sin(\phi_1 - \phi_2) - \frac{1}{4}\sin(\phi_1 + \phi_2 - 2\theta), \tag{2.11a}$$

$$\dot{p}_{\phi_2} = -\partial_{\phi_2} H = \frac{1}{12}\sin(\phi_1 - \phi_2) - \frac{1}{4}\sin(\phi_1 + \phi_2 - 2\theta), \tag{2.11b}$$

$$\dot{p}_{\theta} = -\partial_{\theta} H = \frac{1}{2}\sin(\phi_1 + \phi_2 - 2\theta), \tag{2.11c}$$

$$\dot{p}_r = -\partial_r H = 2p_\theta^2 r^{-3} - \left[\frac{1}{4}\cos(\phi_1 - \phi_2) + \frac{3}{4}\cos(\phi_1 + \phi_2 - 2\theta)\right] r^{-4} + F_C. \tag{2.11d}$$

Inspecting Eq. (2.11c) we see immediately that the orbital momentum, p_θ, is static if and only if $\phi_1 + \phi_2 - 2\theta = j\pi$ where j is any integer. Using that as a constraint we then see that both spin momenta are static if the previous equation holds and $\phi_1 - \phi_2 = k\pi$ where k is an integer independent of j. These two constraints produce a set of equilibrium curves where

$$\phi_1 = \frac{j+k}{2}\pi + \theta, \tag{2.12a}$$

$$\phi_2 = \frac{j-k}{2}\pi + \theta, \tag{2.12b}$$

and all the forces on the three angular momenta are 0. However since our Hamiltonian is periodic over 2π we can cover everything by permuting (j, k) through 0 and 1. This leaves us with 4 curves, until we consider the constraint that Eq. (2.11d) must be negative to maintain contact. If j is odd, then we're left with a resulting positive radial force of $1/2$, and we lose contact. So we've narrowed down from an infinite number of equilibrium curves to two, which, using the j-k notation are (0,0) and (0,1). These curves correspond with the continuous ground states Schönke [15] found despite not fixing the dipoles to rotate in place.

Normal Mode Analysis

Equilibria and equations of motion in hand, we can do small angle perturbations. Noting that near an equilibrium point $\Gamma_i = (\phi_{1i}, \phi_{2i}, \theta_i, p_{\phi_{1i}}, p_{\phi_{2i}}, p_{\theta_i}) = (\phi_{1i}, \phi_{2i}, \theta_i, 0, 0, 0)$

the changes in momenta will be small. Doing a Taylor approximation around these equilibria points as described in the introduction section on higher dimension linearization[1.2.5] we find $\widehat{P}$ matrices for each of the equilibria.

For the (0,0) equilibrium we find the perturbation matrix to be

$$\begin{bmatrix} \frac{\omega^2}{10} - \frac{1}{3} & -\frac{1}{6} & \frac{1}{2} \\ -\frac{1}{6} & \frac{\omega^2}{10} - \frac{1}{3} & \frac{1}{2} \\ \frac{1}{2} & \frac{1}{2} & \frac{\omega^2}{2} - 1 \end{bmatrix} \tag{2.13}$$

Which only has two non-zero eigenmodes corresponding to when ω^2 is equal to 5/3 and 7. The lower frequency mode has an eigenvector of [1, -1, 0], indicating it has no motion in the orbital angle, θ. For this reason we shall refer to it as the spinning mode for its sole form of motion. It possesses an interesting isomorphism we shall examine in more depth later. The second, higher, frequency's eigenvector is [5/2, 5/2, -1] indicating it does possess orbital motion and thus earns the moniker of orbital mode. These modes correspond to the α and β modes in Pollack [2] respectively. The spinning mode matches α exactly. Allowing for θ to be dynamical appears to result in a higher restoring force as the frequency is higher than is the case with β. Brief algebra will reveal that both modes have net-0 angular momentum.

Additionally this result along with the work Stump did on radiation damping of oscillating dipoles [16] lets us estimate the significance of that phenomenon on this system. When approximating the damping effect as producing an exponential decay the oscillations have a time constant, that when expressed in our units, is

$$\tau_{decay} = 180c^3 \left(L_0^2 \omega_0^2 \frac{L_0}{T_0} \right)^{-1} T_0. \tag{2.14}$$

This means for reasonably sized dipoles (dipole moment of 0.5 $\mathrm{H/m^2}$ and diameter of 0.01 m) we would observe an enormous amount of oscillations before any significant energy was lost to simple dipole radiation, on the order of several life times of the universe; $\tau_{decay} \approx 10^{20}$ years. Other forms of dissipation would almost certainly dominate.

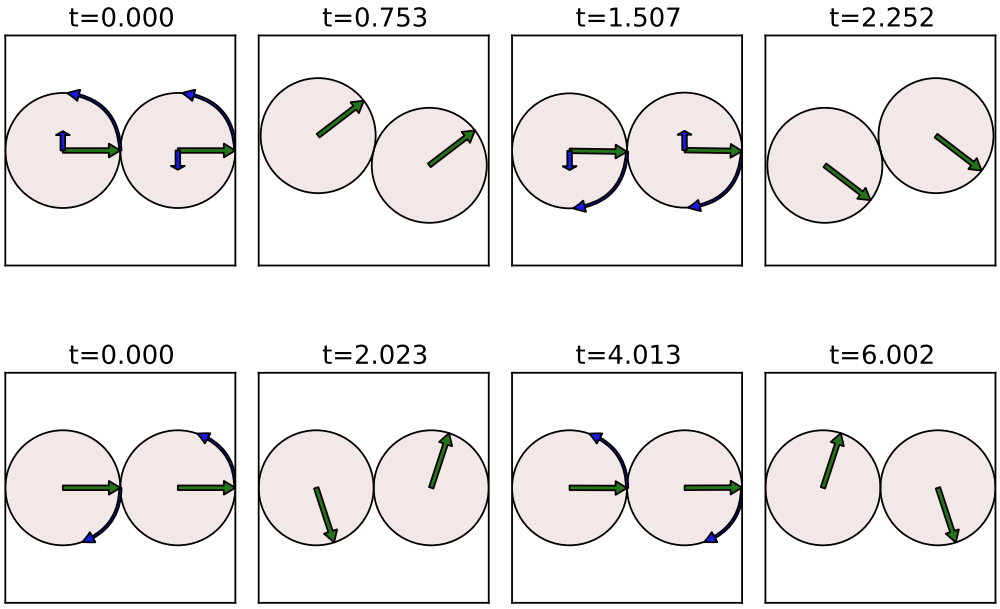

Figure 2.2: Numerical results for four frames of an orbital mode with period 3 (top row), and a spinning mode with period 8 (bottom row). Color editions have blue arrows denoting velocities, with green arrows denoting dipole orientations.

For the (0,1) equilibrium the perturbation matrix is

$$\begin{bmatrix} \frac{\omega^2}{10} - \frac{1}{6} & -\frac{1}{3} & \frac{1}{2} \\ -\frac{1}{3} & \frac{\omega^2}{10} - \frac{1}{6} & \frac{1}{2} \\ \frac{1}{2} & \frac{1}{2} & \frac{\omega^2}{2} - 1 \end{bmatrix} \tag{2.15}$$

Which merits two points of observation. First, all the same eigenvectors come forth along with 2 non-zero fundamental frequencies. Second, while the orbital mode has the same frequency, the spinning mode's $\omega^2 = -5/3$. It follows then that the frequency has a negative complex component. When that frequency is put back into the periodic solution of $e^{i\omega t}$ we'll have a growing exponential indicating that it is unstable.

Both the (0,0) and (0,1) equilibria points have an $\omega^2 = 0$ mode where all the angles have been translated by some equal amount. With all the translation being the same, there's

no restoring force and thus no oscillation.

Isomorphisms

Examining the spinning mode in more depth we present the variable substitution for the difference and sum of the dipole orientations and corresponding velocity

$$\phi_d = \phi_1 - \phi_2 \tag{2.16a}$$

$$\phi_t = \phi_1 + \phi_2 \tag{2.16b}$$

$$\dot{\phi}_d = \dot{\phi}_1 - \dot{\phi}_2 \tag{2.16c}$$

$$\dot{\phi}_t = \dot{\phi}_1 + \dot{\phi}_2 \tag{2.16d}$$

Making these substitutions in the original Lagrangian we find new momenta and a new Hamiltonian. The momenta are $p_{\phi_d} = \dot{\phi}_d/20$ and $p_{\phi_t} = \dot{\phi}_t/20$ while the contact Hamiltonian in these coordinates is

$$\begin{aligned} H = T + U = \frac{1}{2}\left(2p_\theta^2 + 20p_{\phi_d}^2 + 20p_{\phi_t}^2\right) \\ - \frac{1}{12}[\cos\phi_d + 3\cos(\phi_t - 2\theta)] \end{aligned} \tag{2.17}$$

Let us consider just the spinning mode with $\phi_t = \theta = p_{\phi_t} = p_\theta = 0$. Using this Hamiltonian it becomes clear that when those four variables all start at 0 they stay at 0, reducing this phase space from 6 dimensions to 2.

$$H_{\phi_d} = 10p_{\phi_d}^2 - \frac{1}{12}\cos\phi_d \tag{2.18}$$

It is important to note the similarities of this Hamiltonian with the Hamiltonian for a simple pendulum. As is the case for a pendulum, the Hamilton equations lead us to a second order differential equation $\ddot{\phi}_d = -\frac{5}{3}\sin\phi_d$ providing a second check that the small amplitude frequency is correct. The large amplitude period is not expressible in terms of an elementary function, but is expressible in terms of an elliptic integral of the first kind.

Coupling

Considering now the Hamiltonian for the other two angles we have

$$H_{\phi_t,\theta} = \frac{1}{2}\left(2p_\theta^2 + 20p_{\phi_t}^2\right) - \frac{1}{12}[3\cos(\phi_t - 2\theta)], \tag{2.19}$$

which holds while the contact criterion is observed.

$$-\partial_{\phi_t} H = \dot{p}_{\phi_t} = -\frac{1}{4}\sin(\phi_t - 2\theta) \tag{2.20a}$$

$$-\partial_\theta H = \dot{p}_\theta = \frac{1}{2}\sin(\phi_t - 2\theta) = -2\dot{p}_{\phi_t} \tag{2.20b}$$

$$\partial_{p_{\phi_t}} H = \dot{\phi}_t = 20p_{\phi_t} \tag{2.20c}$$

$$\partial_{p_\theta} H = \dot{\theta} = 2p_\theta \tag{2.20d}$$

The rates of change for the momenta (Eq. 2.20b plus two times Eq. 2.20a equals zero) clearly denote a conserved quantity we'll call total angular momentum and denote as $L_\mathrm{t} = p_\theta + 2p_{\phi_t}$. This is to be expected as the angular components only appear in the Hamiltonian together in a single periodic function. With this we can produce the expression

$$\begin{aligned}\phi_t(t) = \phi_{t0} + \int_0^t \dot{\phi}_t dt = \phi_{t0} + \int_0^t 20p_{\phi_t} dt = \phi_{t0} + \int_0^t 10(L_\mathrm{t} - p_\theta)dt \\ = \phi_{t0} + 10L_\mathrm{t}t - 10\int_0^t p_\theta dt.\end{aligned}, \tag{2.21}$$

which we'll rearrange to get

$$\int_0^t p_\theta dt = L_\mathrm{t}t + (\phi_{t0} - \phi_t(t))/10. \tag{2.22}$$

A similar integral can be set up for θ

$$\begin{aligned}\theta(t) = \theta_0 + \int_0^t \dot{\theta} dt = \theta_0 + \int_0^t 2p_\theta dt \\ \int_0^t p_\theta dt = \frac{1}{2}[\theta(t) - \theta_0].\end{aligned} \tag{2.23}$$

While the integral of p_θ is not analytic, the equality between the two holds while contact is maintained which allows us to algebraically rearrange Eq. (2.22) and Eq. (2.23) to get

$$\phi_t(t) = -5\left[\theta(t) - \theta_0 - \frac{1}{5}\phi_{t0}\right] + 10L_{\mathrm{t}}t. \tag{2.24}$$

Considering the force on p_θ from Eq. (2.20b) and making this new substitution starting from equilibrium and a zero angular momentum starting condition we have

$$\ddot{\theta} = \sin(-5\theta - 2\theta) = -\sin 7\theta \approx -7\theta \tag{2.25}$$

And doing the same with p_{ϕ_t} from Eq. (2.20a) produces

$$\ddot{\phi}_t = -\frac{20}{4}\sin(\phi_t + \frac{2}{5}\phi_t) = -5\sin\left(\frac{7}{5}\phi_t\right) \approx -7\phi_t, \tag{2.26}$$

showing that while the contact constraint holds, the orbital state is also isomorphic with the simple pendulum with the same asymptotic behavior as the small amplitude oscillations we found earlier. With this we see that when $L_{\mathrm{t}} = 0$ and contact maintained we have reduced the problem to two independent pendula. While the periods are independent of each other and unlikely to form a rational fraction, both are periodic. This fact makes the system as a whole no more complicated than quasi-periodic.

2.3.2 Numerical Results

Method

An adaptive fourth order Runge-Kutta method was implemented to calculate the trajectory of the system using two different sized time steps, both made smaller until they agreed within a specified precision. To determine if a trajectory has returned through its original point in phase space $\mathbf{\Gamma}(0) = \mathbf{\Gamma}_0$ linear interpolation was used between steps $\mathbf{\Gamma}_n$ and $\mathbf{\Gamma}_{n+1}$ to get an estimated time for when the initial value was revisited. This generated six estimated recurrence times. If all six calculated values fell between t_n and t_{n+1} the average

was taken and stored. This process was continued until 75 time units had elapsed. The stored recurrence times were fit to the equation $t_m = t_0 m$ where m is an integer. The slope t_0 was taken to be the period.

Period versus Energy curves

The spinning and orbital modes were examined independently as they are not coupled together when the contact criterion is maintained. Two hundred initial conditions were simulated with closer resolution taken near transition points. In the case of the spinning mode, the maximum initial kinetic energy was 1/2, taking it well past the point where it begins spinning freely. We see that its period as a function of energy reproduces the curve described in a detailed analysis of the basic pendulum [17]. In the case of the orbital mode, the maximum energy was just below the point where the contact criterion was broken, 1/3 units of initial kinetic energy.

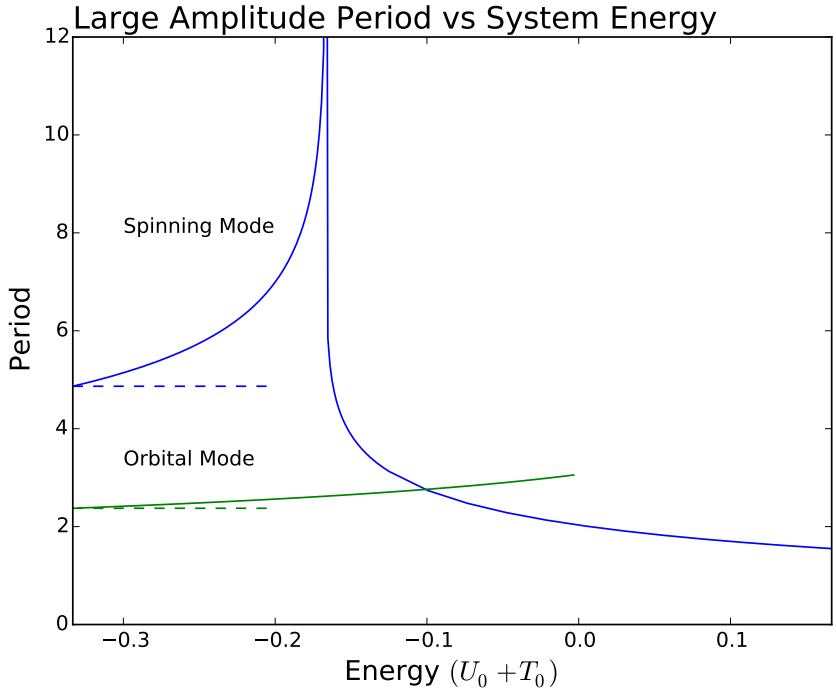

Figure 2.3: Above is a plot of large amplitude period vs. total system energy. Solid lines denote numerical results, dashed lines denote asymptotic small amplitude limit

2.4 Conclusions

In the analysis of this system so far we have found an interesting example of a coupled non-linear Hamiltonian that counter intuitively does not produce chaotic motion. However this is only the first of many questions this system leaves open for discussion. Using equation Eq. (2.9) we can ask whether this splitting of the Hamiltonian works for any set of spheres or if there are certain ratios that must hold. We can also explore stability of circular orbits that likely exist. With the appropriate numerical techniques we can examine how these spheres interact with bouncing. These questions and more are available for investigation.

CHAPTER 3

Hysteresis in A System of Seven Magnets

3.1 Introduction

Having examined the twin dipole system in more depth, one of the things that intrigued me was the work by Stump et al. [3] on magnets arranged in a polygon and how it would change under different circumstances. An easy experiment would ask how does the system react to changes. The hexagonal system would be very easily modified by introducing a seventh in the center. This is trivial to do with off-the-shelf toy magnets and making an approximate system with variable strength electromagnets is also within the realm of the imaginable. This motivates the theoretical work that follows.

We consider a system of six identical dipoles at the vertices of a regular hexagon and a seventh dipole fixed at the center identical to the other six except that its dipole strength is variable. All seven are constrained to spin frictionlessly on axes so their dipole moments remain coplanar with the hexagon. To find equilibrium states, we begin with the solution of Stump et al. [3], which is applicable for a central dipole of zero strength. We then construct equilibrium states for finite central dipole strength by increasing the central dipole strength incrementally and introducing an effective drag in Lagrange's equations to enable the system to relax until the net torque on each dipole vanishes. These states agree with those obtained by Smith et al. [18] by minimizing the magnetostatic potential energy. We explore normal modes of oscillation by considering small-amplitude periodic perturbations about these states.

Two qualitatively different overlapping regimes of oscillatory motion are observed with discontinuous transitions at critical values of the central dipole strength. These critical values agree with those found by Smith et al. [18] by considering transitions in the magnetostatic potential energy. For vanishing central dipole strength, our numerical results agree

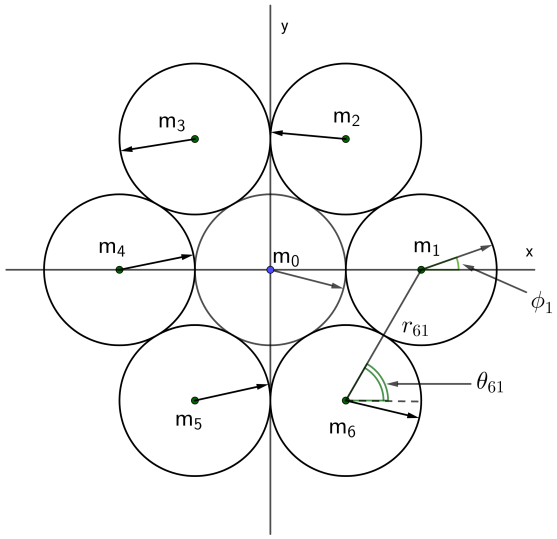

Figure 3.1: Diagram depicting six dipoles arranged at the vertices of a regular hexagon with a seventh dipole at the center. Dipole orientations are denoted by arrows, with ϕ_i denoting the angle that dipole i makes with the x-axis. The distance between dipoles i and j is denoted by r_{ij}. The angle that segment r_{ij} makes with the x-axis is denoted by θ_{ij}. The perimeter dipoles $m_1, m_2, ..., m_6$ all have the same strength m, while the central dipole may have a different strength, m_0.

with analytical calculations by Stump et al. [3]. At very large values of the central dipole strength, our numerical results converge to our analytical calculations for an infinitely strong central dipole.

3.2 System And Methods

3.2.1 Geometry

The centers of six identical dipoles are fixed at the vertices of a hexagon, and a seventh dipole with variable strength but identical moment of inertia is fixed at the center of the hexagon. All seven are allowed to spin freely in the plane of the hexagon about axes that are perpendicular to this plane, with their magnetic moments directed parallel to this plane. The ith dipole's orientation relative to the x-axis is denoted as ϕ_i, with $i = 0, 1, 2, ..., 6$. The distance between dipoles i and j is denoted as r_{ij} and the angle of the associated line segment with the x-axis is denoted as θ_{ij} (Fig. 3.1).

3.2.2 Equations of Motion

We start with the magnetostatic potential energy of a pair of magnetic dipoles as described in the introduction 1.2 with some modifications and algebraic simplifications [19],

$$U_{ij} = -U_0 \frac{C_{ij}}{2} \left(\frac{a}{r_{ij}} \right)^3 [\cos(\phi_i - \phi_j) \tag{3.1}$$

$$+ 3\cos(\phi_i + \phi_j - 2\theta_{ij})]. \tag{3.2}$$

Here,

$$U_0 = \frac{\mu_0 m^2}{4\pi a^3} \tag{3.3}$$

is the energy scale, μ_0 is the vacuum permeability, m is the strength of a perimeter dipole, and a is the distance between adjacent dipole centers. The coefficient is

$$C_{ij} = \begin{cases} \alpha \text{ if } i = 0 \text{ or } j = 0 \\ 1 \text{ otherwise} \end{cases} \tag{3.4}$$

involves the ratio $\alpha = m_0/m$ of the central dipole strength m_0 to the perimeter dipole strength m. The limiting case illustrated in Fig. 3.1 shows $a = D$, the sphere diameter. Our calculations are also valid for $a > D$, which would apply if the dipoles were kept a fixed distance from each other by some other force. The total magnetostatic potential energy of the system is given by

$$U(\vec{\phi}) = \frac{1}{2} \Sigma_{i,j=0,i\neq j}^{6} U_{ij}, \tag{3.5}$$

where the factor $1/2$ ensures that each pairwise interaction is counted only once. The total kinetic energy is

$$T = \frac{I}{2} \Sigma_i \dot{\phi}_i^2, \tag{3.6}$$

where I is the moment of inertia of a dipole. The Lagrangian and equations of motion are

$$L = T - U \tag{3.7a}$$

$$\frac{d}{dt}\left(\partial_{\dot{\phi}_i} L\right) = \partial_{\phi_i} L \tag{3.7b}$$

$$I\ddot{\phi}_i = -\partial_{\phi_i} U, \tag{3.7c}$$

where $\partial_{\phi_i} = \partial/\partial\phi_i$. To determine equilibrium states, we begin with the ground state of orientations found in Stump et al. [3] for hexagonally arranged dipoles and increase α incrementally from $\alpha = 0$. Increasing α generally drives the system out of equilibrium, and integrating Eqs. (3.7c) leads to undamped oscillations about some new equilibrium state. We use an RK45 numerical integrator [20] to evolve the system in time. To damp these oscillations and settle into the new equilibrium, we slowly increase a damping factor γ to dissipate energy,

$$I\ddot{\phi}_i = -\partial_{\phi_i} U - \gamma\dot{\phi}_i. \tag{3.8}$$

The objective is to pass through critical damping and to reduce the sum of the squares of the accelerations until this sum is below a small threshold ϵ,

$$\Sigma_{i=0}^{6}\ddot{\phi}_i^2 < \epsilon. \tag{3.9}$$

For most of the simulations, we use $\epsilon = 10^{-8}$. Once this threshold is reached we consider the configuration to be an equilibrium state, $\vec{\phi}^*(\alpha)$.

These equilibrium states agree with those obtained by minimizing the magnetostatic potential energy [18]. The total system's net dipole moment and potential energy undergo a bifurcation at a critical value $\alpha = \alpha_2 \approx 2.47$, above which the central magnet plays a dominant role. We therefore refer to this state as the "dipole state". When lowering α through α_2, the dipole state persists until a lower critical value $\alpha = \alpha_1 \approx 1.16$ is reached, below which the system reverts to the original state, called the "circular state" because because

of the significant role of the perimeter magnets. Thus, the system possesses hysteresis.

With equilibrium states in hand we can use the linearization process described in section [1.2.5] to find the eigenstates. It is slightly easier than Eq. [1.13] as all our mass terms are identical and the matrix capturing them behaves as a scalar. We also take advantage of having bundled all our units for potential energy into a leading term to produce

$$\frac{-\omega_i^2}{\Omega^2}\delta\vec{\phi}_i = \widehat{K}\delta\vec{\phi}_i, \tag{3.10}$$

where the elements of $\widehat{K}$ are defined by

$$K_{ij} = -\left(\partial_{\phi_j}\partial_{\phi_i}\frac{U}{U_0}\right)\Bigg|_{\vec{\phi}^*}. \tag{3.11}$$

These are evaluated numerically. The characteristic frequency is defined by

$$\Omega^2 = \frac{U_0}{I} \tag{3.12}$$

and is the same used in Stump [3].

3.3 Analysis

3.3.1 Comparing with Prior Results

The $\alpha = 0$ case provides an opportunity to validate our method by comparing it with the magnetic polygon analysis of Stump et al. [3], as our $\alpha = 0$ case is equivalent to their $N = 6$ case. For N magnets located at the vertices of a regular N-gon, their normal-mode frequencies are given by

$$\omega_j^2 = \Omega^2\left(Z_N + \Sigma_{\nu=1}^{N-1}\left[\frac{1+\sin^2\frac{\pi\nu}{N}}{\rho(\nu)}\right]\cos\frac{2\pi}{N}j\nu\right). \tag{3.13}$$

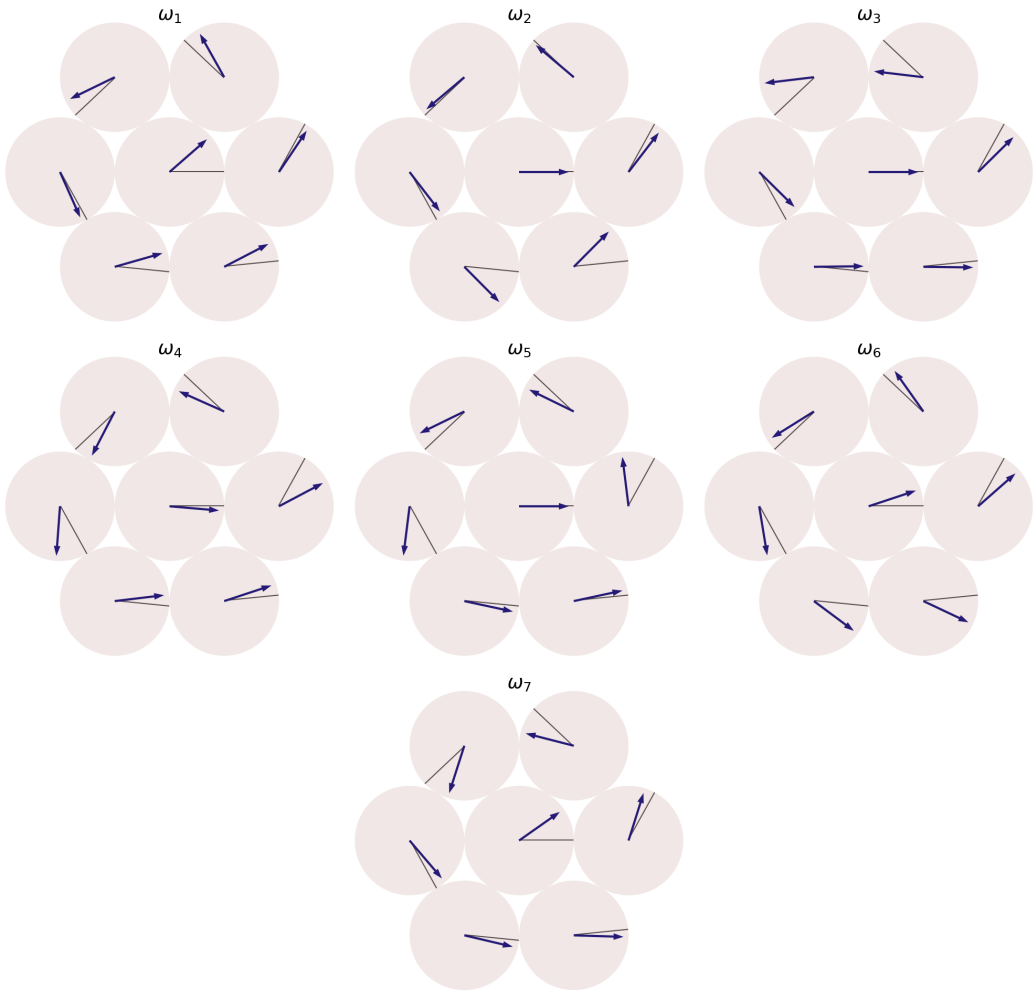

Figure 3.2: Schematic representations of the seven eigenmodes of oscillation about the circular state for a central dipole with relative strength $\alpha = 1.3$. The thin lines denote the equilibrium dipole orientations for this configuration, $\vec{\phi}^*$. The arrows denote the perturbed orientations, $\vec{\phi}^* + \delta\vec{\phi}_i$.

Here j is the mode label ranging from 1 to 6,

$$\rho(n) = \frac{\sin(\pi n/N)}{\sin(\pi/N)} \tag{3.14}$$

is the dimensionless distance between a pair of dipoles, and

$$Z_N = \Sigma_{n=1}^{N-1} \frac{1 + \cos(\pi n/N)^2}{\rho(n)^3} \tag{3.15}$$

is a quantity related to the potential energy per dipole,

When $N = 6$ there are four unique eigenvalues. To account for scaling factors, we compare the ratios in rising order, ω_2^2/ω_1^2 and so on. Since there are four unique eigenvalues, there will be three such ratios. To six decimals, they are 1.364407, 1.722194, and 1.578773. The values generated by our methodology agree within machine precision(1 part in 10^{14}). A seventh mode exists in our system associated with the free spinning of the central magnet, as at $\alpha = 0$ the central magnet is uncoupled to the orientation of the six perimeter magnets.

3.3.2 Normal Modes of Oscillation

Figure 3.2 shows the normal modes of oscilllation about the circular state for $\alpha = 1.3$. Using Eq. (3.10) to evaluate the normal modes as a function of α, we obtain Figs. 3.3 and 3.4. These plots allow us to survey the behavior of the normal modes over the full range of the circular state.

One noteworthy feature in Fig. 3.3a is the splitting from four distinct modes at $\alpha = 0$, two of which are doubly-degenerate, to six distinct modes for $\alpha > 0$. Additionally, a new eigenmode (ω_1) associated with movement of the central magnet appears, and its frequency eventually surpasses the next lowest and briefly the third lowest.

The frequencies vary continuously throughout the process until $\alpha = \alpha_2$, where the circular state equilibrium becomes unstable. This and characteristic ratios between different coordinates that remain constant provides a consistent way to identify each mode. For example, in mode 1, $\delta\phi_1/\delta\phi_4 > 0$ so if you were calculating normal modes and unsure if a

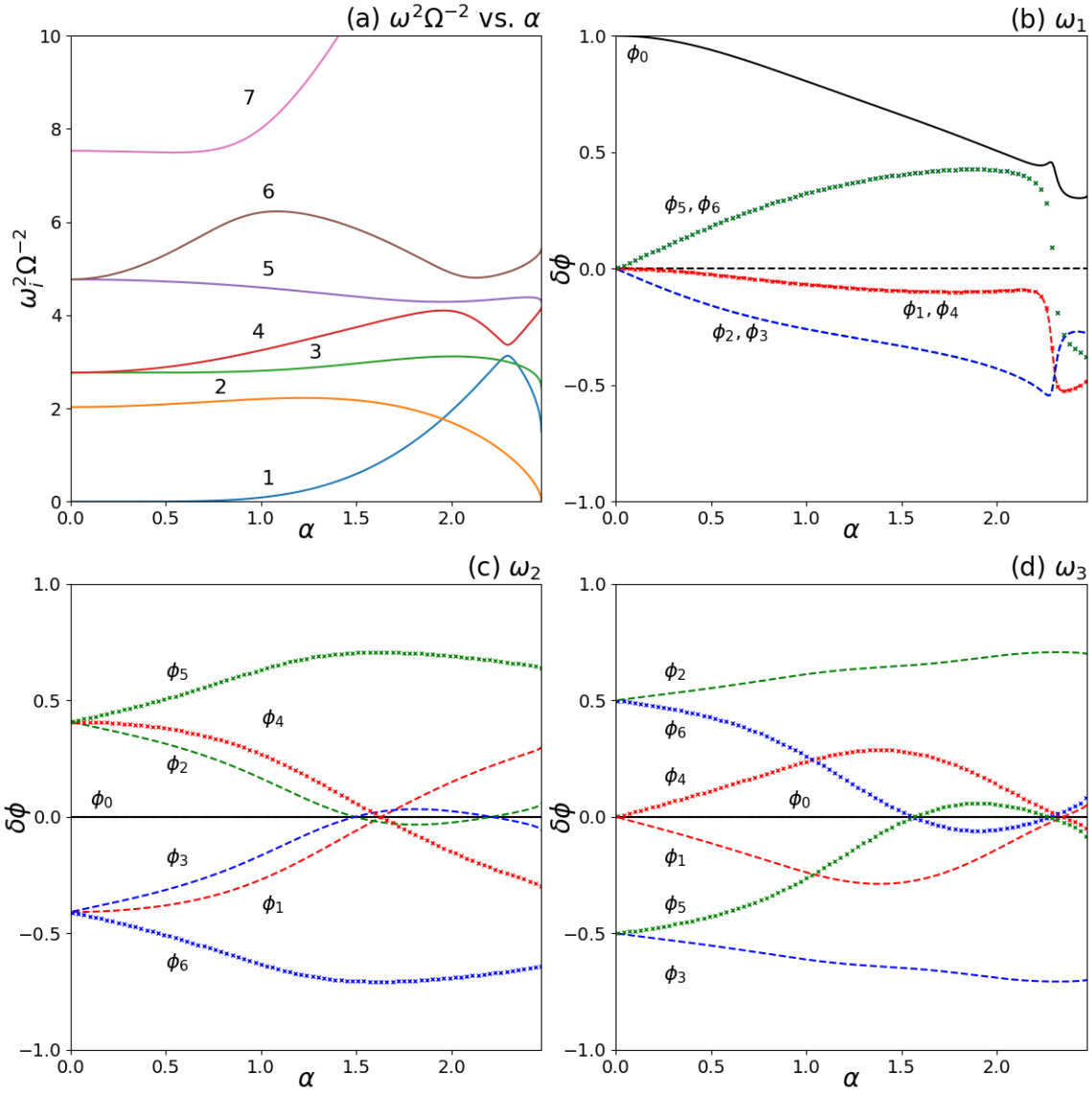

Figure 3.3: Panel (a) is the eigenvalue ω^2 vs. α for each of the seven modes of oscillation about the circular state, labeled based on ascending order at $\alpha = 0$. Panels (b) through (d) are plots of the vectors of oscillation about the circular state, $\delta\vec{\phi}$ For modes 1-3. Dashed traces correspond to ϕ_1,ϕ_2 and ϕ_3, while the thicker markers correspond to ϕ_4, ϕ_5 and ϕ_6. The solid trace denotes the value of ϕ_0. In many cases two degrees of freedom are synchronized, in which case the variables are listed as a comma-separated pair.

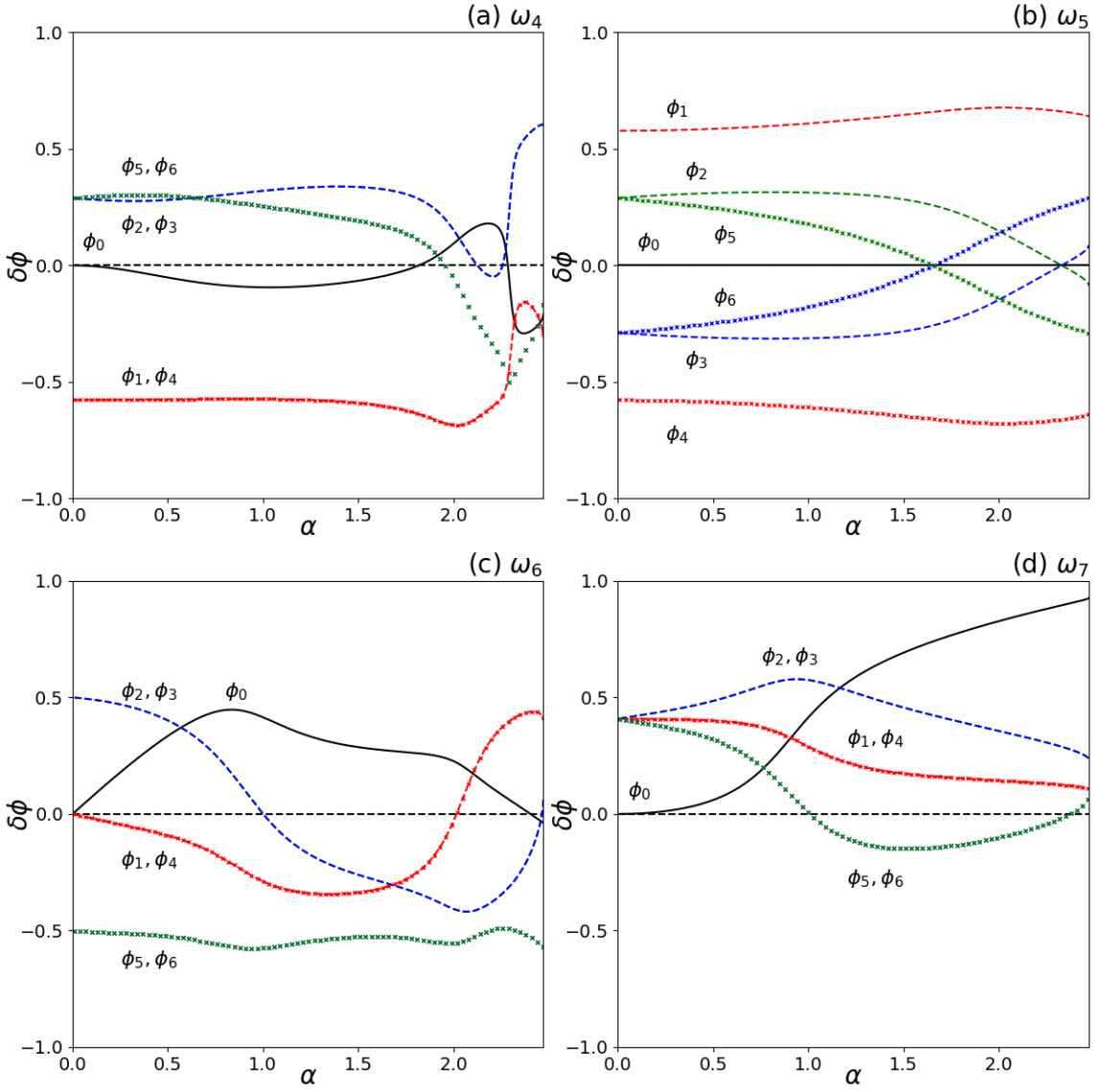

Figure 3.4: Panels (a) through (d) are the vectors corresponding to modes 4 through 7 about the circular state. Labeling is the same as for panels (b) through (d) described in Fig. 3.3.

vector was associated with mode 1, 2, or 3, calculating $\delta\phi_1/\delta\phi_4$ would tell you if you had mode 1, or either mode 2 or 3.

3.3.3 Large α Limit

One of the difficulties in developing an analytic method for calculating the eigenmodes of this system is that it is hard to solve the nonlinear forces and find the system's equilibria. However, there are two values of α where the calculation is simple. Stump et al. [3] has already examined $\alpha = 0$, as was mentioned earlier, exploiting the system's strong symmetry to determine the equilibrium. The other such case is $\alpha = \infty$. As α increases, the perimeter magnets will increasingly align with the field of the central magnet. At the extreme limit, all other interactions will be swamped by the central magnet's field. From this we know that

$$\hat{m}_i \parallel \mathbf{B}_0 \parallel \left(2\cos^2\theta_{0i} - \sin^2\theta_{0i}\right)\hat{x} + 3\cos(\theta_{0i})\sin(\theta_{0i})\hat{y}, \tag{3.16}$$

where θ_{0i} is the angle defined in Sec. 3.2.1 and $\mathbf{B}_0$ is the magnetic field generated by the central dipole at that location. For $i = 1, 2, ..., 6$, these equilibrium angles are [18] $0,\ \pi - \tan^{-1}(3^{3/2}),\ \tan^{-1}(3^{3/2}) - \pi,\ 0,\ \pi - \tan^{-1}(3^{3/2}),\ \tan^{-1}(3^{3/2}) - \pi$. Specifying these angles allows us to evaluate the elements of the linearization matrix $\widehat{K}$ in a known configuration.

It works out that $\widehat{K}$ contains terms of α to at most the first power, and is analogous to the spring constant k in a simple harmonic oscillator. As α approaches infinity, all ω_i^2 would also approach infinity. For this reason we will actually calculate the matrix $\lim_{\alpha\to\infty}(\widehat{K}/\alpha)$ which is presented here to 4 decimal places:

$$\begin{bmatrix} -9.2915 & -1.0 & -1.5118 & -1.5118 & -1.0 & -1.5118 & -1.5118 \\ -1.0 & -2.0 & 0 & 0 & 0 & 0 & 0 \\ -1.5118 & 0 & -1.3228 & 0 & 0 & 0 & 0 \\ -1.5118 & 0 & 0 & -1.3228 & 0 & 0 & 0 \\ -1.0 & 0 & 0 & 0 & -2.0 & 0 & 0 \\ -1.5118 & 0 & 0 & 0 & 0 & -1.3228 & 0 \\ -1.5118 & 0 & 0 & 0 & 0 & 0 & -1.3228 \end{bmatrix}, \tag{3.17}$$

for which computer algebra systems [21] can readily determine the eigenvalues. These values correspond to $-\omega_i^2/\Omega^2\alpha$ and are, to 4 decimal places, -0.1815, -1.3229, -1.9126, -2.0000, and -10.5203. The second-lowest mode is triply degenerate. We will refer to these as Ω_i^2 where

$$\lim_{\alpha\to\infty} \frac{\omega_i^2}{\Omega^2\alpha} = \Omega_i^2. \tag{3.18}$$

To compare Ω_i with the normal modes of the system at other values of α we define a ratio,

$$R_i = \frac{\omega_i^2}{\alpha\Omega^2}\frac{1}{\Omega_i^2}, \tag{3.19}$$

that captures how close a mode's eigenvalue matches its limiting behavior, with 1 being an exact match. Figure 3.5 is a plot of R_i vs. $1/\alpha$.

The limiting behavior in Fig. 3.5 for $\alpha \to \infty$ supports the claim that the process used for intermediate values is sound. The values for the eigenvalues and corresponding modes are produced much like the circular state and are presented in Fig. 3.6 and Fig. 3.7. One point of interest is that ω_1^2 approaches 0 at $\alpha \approx 2.07$ before rebounding and then surpassing the value of ω_2^2 which falls and goes negative at the transition point. One contribution to this phenomenon is that at this value the perimeter dipoles are all moving in synchronous in such a way that the magnetic field at the origin tracks the movement of the central dipole in this mode. This behavior has parallels to the transition from the circular state to the dipole state. Another point of interest is the varying rates of convergence on the extremal

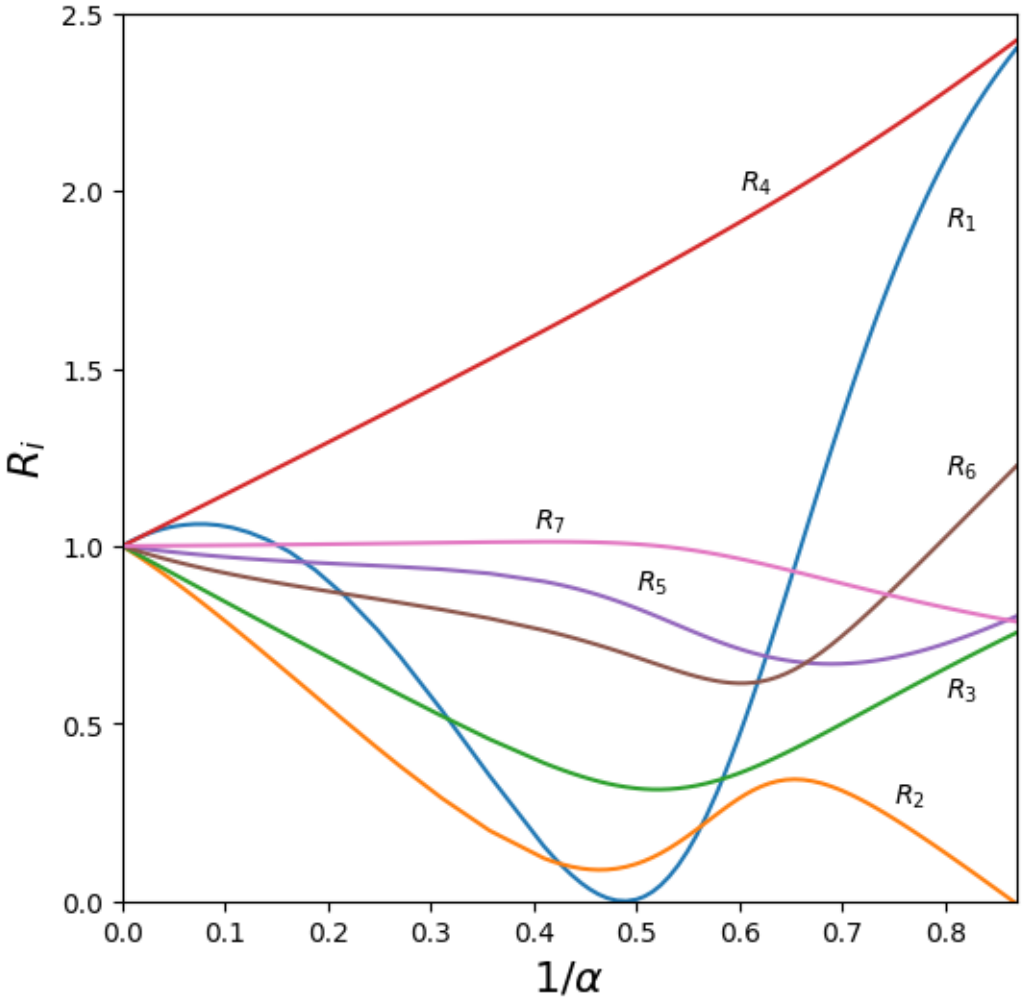

Figure 3.5: R_i is the ratio of eigenvalue ω_i^2/α at α and its projected value for $\alpha \to \infty$, Ω_i. All modes of the dipolar state converge on their $\alpha \to \infty$ limiting behavior at varying rates.

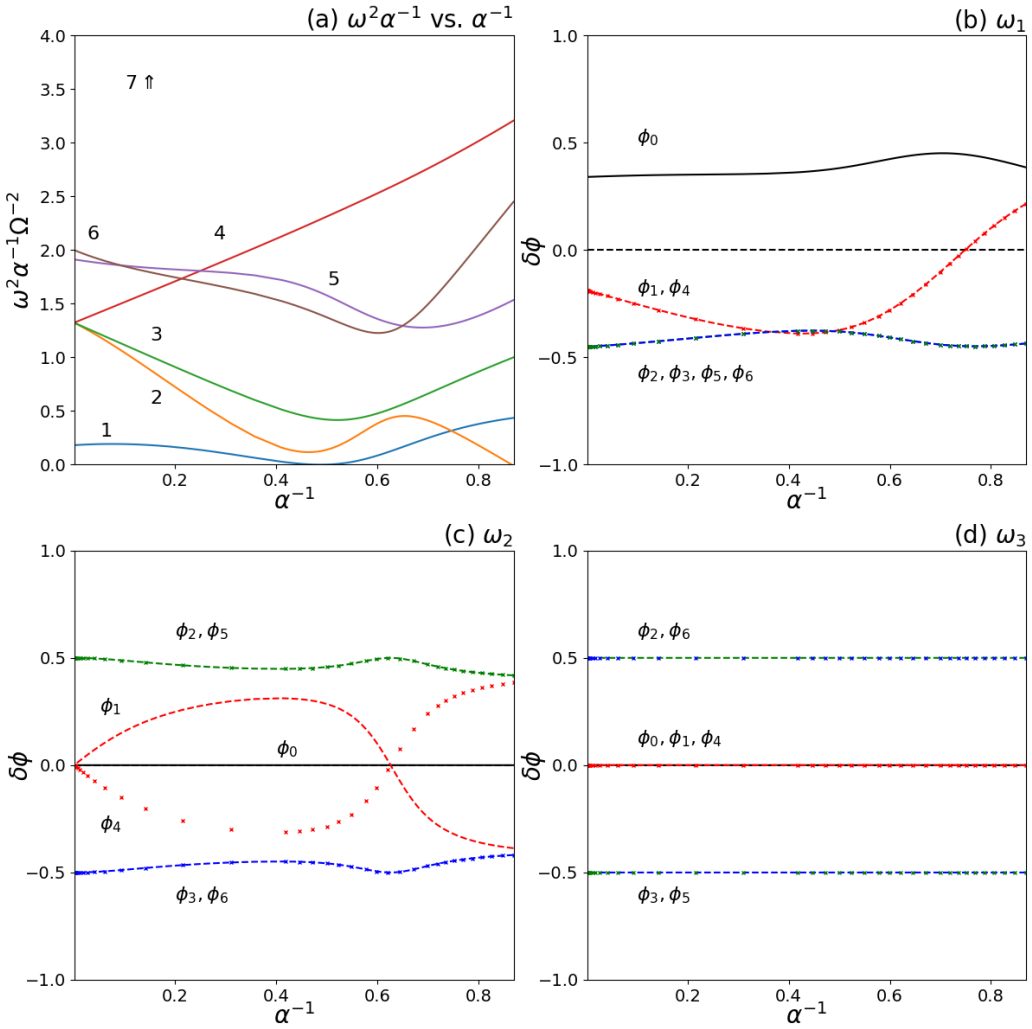

Figure 3.6: Panel (a) is $\omega^2\alpha^{-1}$ vs. α^{-1} while panels (b) through (d) depict the vectors corresponding to the perturbations of the first three modes in the dipole state presented in the same fashion as Fig. 3.3. The arrow in panel (a) indicates that ω_7^2 is off the scale relative to the other six.

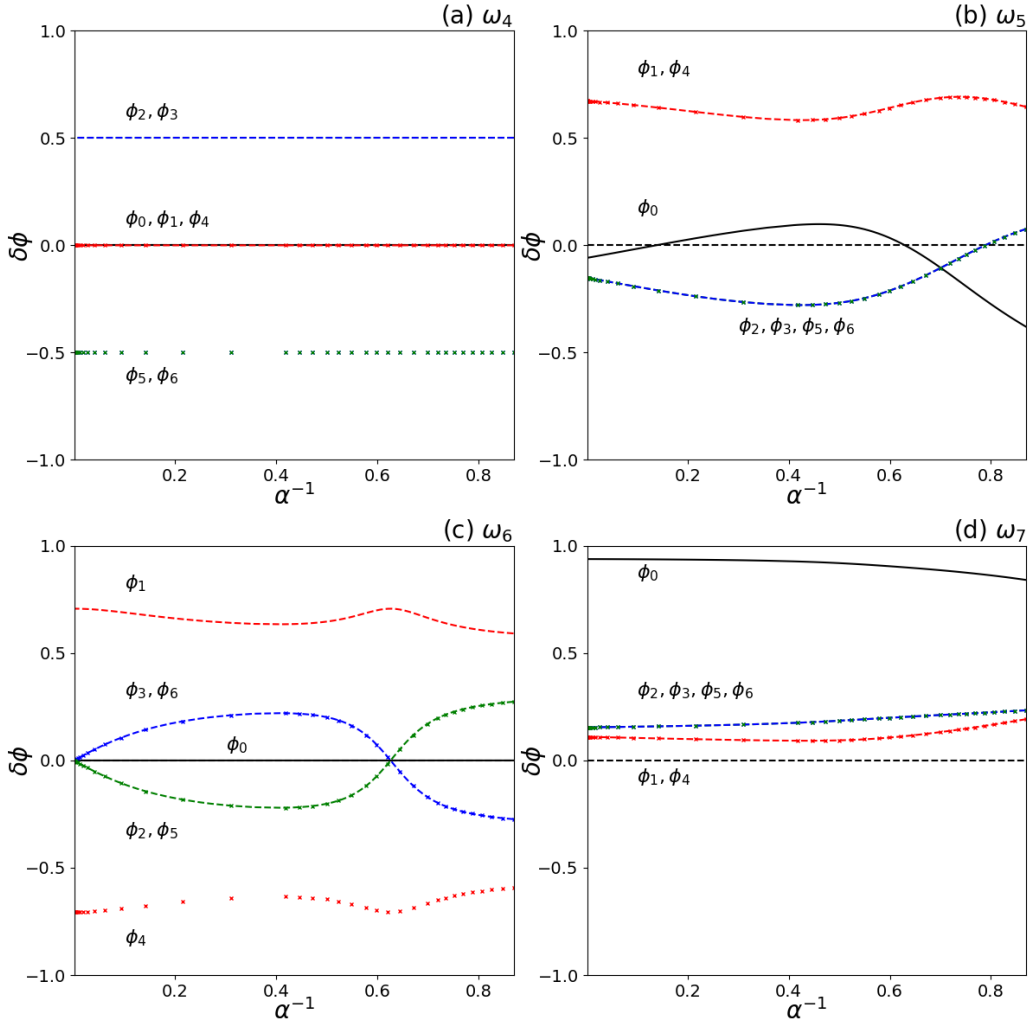

Figure 3.7: Panel (a) through (d) are the perturbations of the remaining four modes in the dipole state presented in the same fashion as Fig. 3.3.

eigenvalues. For example the seventh mode converging quite rapidly while the first mode oscillating substantially.

3.4 Conclusions

A system of seven magnets presents an opportunity to examine bifurcations in a manner that is physically realizable and has few degrees of freedom. The two associated states have qualitatively different normal modes of oscillation and limits. Additionally, the system exhibits hysteresis, transitioning back to the circular state at α_1 which is lower than when it transitions to the dipole state. As a theoretical system, it suggests additional avenues for investigation. What is the simplest configuration of dipoles that can exhibit this behavior? How does the system behave for large N? Insights into the behavior of large collections of dipoles in this configuration may be of application for modeling cylindrical wave guides made of materials with significant molecular dipole moments. This question we will address next.

CHAPTER 4

Base Case for Magnet Systems Exhibiting Hysteresis

4.1 Introduction

When confronted with a new problem or system, it is often useful to identify the simplest case that maintains the basic qualitative properties of interest. Stripping away any extraneous details helps find the parts that are most important and increases your chances at understanding the fundamental "why" of a phenomenon. This is the basic premise when Claude Shannon advocated simplifying a problem to the point where it barely resembled what it looked like when you saw it first. [22]

Before we can identify the simplest system that has the interesting properties of the filled hexagon, we must first identify what those properties are. This will necessarily partially be a matter of aesthetics, but I consider the key properties to be: made up of dipoles spinning in a common plane, with a member varying in strength relative to the others which are all equivalent, that exhibits at least two distinct vibrational mode regimes which overlap, or in other words possesses hysteresis.

We will look at the two dipole system and argue why it can only satisfy the first two and not the latter one. Then we will examine three dipoles arranged in an equilateral triangle and see how they qualitatively behave like the filled hexagon, and what ways they differ quantitatively.

4.2 Why Two Dipoles Are Unremarkable

The interaction between any two dipoles co-aligned in a plane that has been used so far is equation 1.2 and regardless of the coefficient term out front describing the strength of the interaction will always have the same equilibrium where the dipoles are aligned parallel to each other and to the line segment between the two centers. The layout of the potential

energy function won't change as the leading coefficient grows larger, merely steeper. From this we infer that while the frequencies of the two modes described by Pollack would increase, the eigenvectors would not.

4.3 Three Dipoles in a Line

The next step up from two dipoles would be three dipoles, still arranged along a line at equally spaced intervals. This permits us the choice of either placing the varying dipole in the center, producing the potential energy function of

$$\begin{aligned} U_{center} = -\frac{\alpha}{2}\left[\cos\left(\phi_0+\phi_1\right)+3\cos\left(\phi_0+\phi_1\right)+\cos\left(\phi_0-\phi_2\right)+3\cos\left(\phi_0+\phi_2\right)\right] \\ -\frac{1}{16}\cos\left(\phi_1-\phi_2\right)-\frac{3}{16}\cos\left(\phi_1+\phi_2\right), \end{aligned} \tag{4.1}$$

or along the edge

$$\begin{aligned} U_{edge} = -\frac{\alpha}{2}\left(\cos\left(\phi_0-\phi_1\right)+3\cos\left(\phi_0+\phi_1\right)+\frac{1}{8}\cos\left(\phi_1-\phi_2\right)+\frac{3}{8}\cos\left(\phi_1+\phi_2\right)\right) \\ -\frac{1}{2}\cos\left(\phi_0-\phi_2\right)-\frac{3}{2}\cos\left(\phi_0+\phi_2\right). \end{aligned} \tag{4.2}$$

By inspection we see that at equilibrium all the dipoles are aligned with each other ($\phi_0 = \phi_1 = \phi_2 = 0$), and by the same logic in the two dipole case, will continue to be aligned with each other for any value of α we might choose. Because the equilibrium is known for each value of α, the $\widehat{K}$ matrices can be calculated with it included. They are

$$\widehat{K}_{center} = \begin{bmatrix} -4\alpha & -\alpha & -\alpha \\ -\alpha & -2\alpha-\frac{1}{4} & -\frac{1}{8} \\ -\alpha & -\frac{1}{8} & -2\alpha-\frac{1}{4} \end{bmatrix} \tag{4.3}$$

and

$$\widehat{K}_{edge} = \begin{bmatrix} -2\alpha-2 & -\alpha & -1 \\ -\alpha & -\frac{9}{4}\alpha & -\frac{1}{8}\alpha \\ -1 & -\frac{1}{8}\alpha & -\frac{1}{4}\alpha-2 \end{bmatrix}. \tag{4.4}$$

These matrices produce three eigenfrequencies at which these systems oscillate around

Table 4.1: A summary of the eigenfrequencies and how they vary with α in the two cases for a set of three linearly arranged dipoles. Here $F_c = [3(\alpha^2 - \frac{1}{8}\alpha + \frac{3}{256})]^{1/2}$ and $F_e = \frac{3}{2}(\frac{179}{192}\alpha^2 - \frac{3}{4}\alpha + 1)^{1/2}$.

Mode	Center	Edge
ω^2_{slow}	$3\alpha + \frac{3}{16} - F_c(\alpha)$	$\frac{27}{16}\alpha + \frac{3}{2} - F_e(\alpha)$
ω^2_{medium}	$2\alpha + \frac{1}{8}$	$\frac{18}{16}\alpha + 1$
ω^2_{fast}	$3\alpha + \frac{3}{16} + F_c(\alpha)$	$\frac{27}{16}\alpha + \frac{3}{2} + F_e(\alpha)$

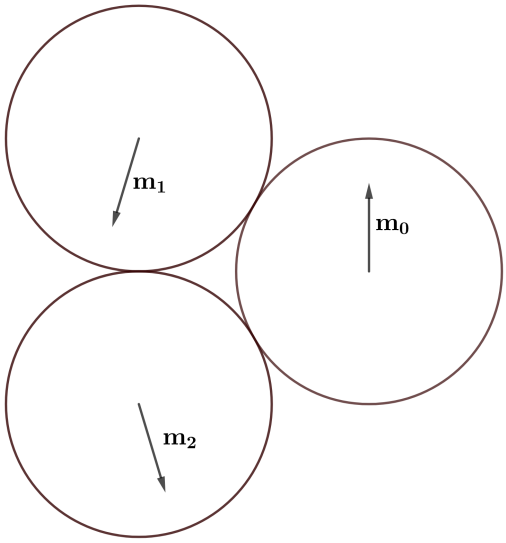

Figure 4.1: Dipoles arranged in an equilateral triangle. A typical configuration for $\alpha < 1$.

their equilibrium. A summary of these curves is presented in table 4.1. The most important result is that these curves are strictly positive for positive values of α, indicating this configuration is stable in that same range and thus doesn't undergo the kind of phase transitions the filled hexagon does. The unexpected result is that for all values of α it holds that $\omega^2_{slow} + \omega^2_{fast} = 3\omega^2_{medium}$. This result holds for other spacings I've looked at.

4.4 The Triangular Case

Having addressed the simpler line cases, I move onto the simplest planar case, an equilateral triangle. For concreteness I place two dipoles on the y axis at $y = \pm 1/2$ and the third variable strength dipole on the x axis at $x = \sqrt{3}/2$, as portrayed in 4.1. The potential

for this system is

$$U(\phi_0,\phi_1,\phi_2) = -\frac{\alpha}{2}\Big[\cos(\phi_0-\phi_1)+\cos(\phi_0-\phi_2) + 3\cos\left(\phi_0+\phi_1+\frac{\pi}{3}\right)+3\cos\left(\phi_0+\phi_2-\frac{\pi}{3}\right)\Big] - \frac{1}{2}\cos(\phi_1-\phi_2)-\frac{3}{2}\cos(\phi_1+\phi_2-\pi). \tag{4.5}$$

Using the same annealing method described in equation 3.8, I arrive at equilibria and normal mode plots as shown in figure 4.2. While less exotic than the filled hexagon system, mode 1 does trend lower hitting 0 and becoming unstable at $\alpha \approx 6.5$. I also note that while there is a degeneracy at $\alpha = 1$, there is only one solution of eigenvectors that would maintain continuous curves.

Starting from the other extreme with very large α and the starting orientations aligned with the field lines generated by the variable dipole we get the curves in figure 4.3. Looking at the high α regime's eigenmodes we see nearly flat lines with the only noteworthy point being that mode 1 becomes unstable at $\alpha \approx 2.47$.

These two results provide evidence that these three dipoles have a low α state and a high α state, two distinct modes of behavior. Furthermore the two states overlap for values of α $2.47 < \alpha < 6.5$ meaning the state of the system depends on its previous condition, or more concisely put, it has hysteresis. Having laid out arguments for why dipoles arranged in a straight line would not, I conclude that the simplest arrangement of dipoles that has hysteresis associated with a variable strength member is the equilateral triangle.

Examining figure 4.4 we see the two states in a more macroscopic comparison of their potential energies at equilibrium. Notice for the bulk of the region where their phases overlap, the low α phase is metastable until it becomes fully unstable and only the high α phase can be maintained.

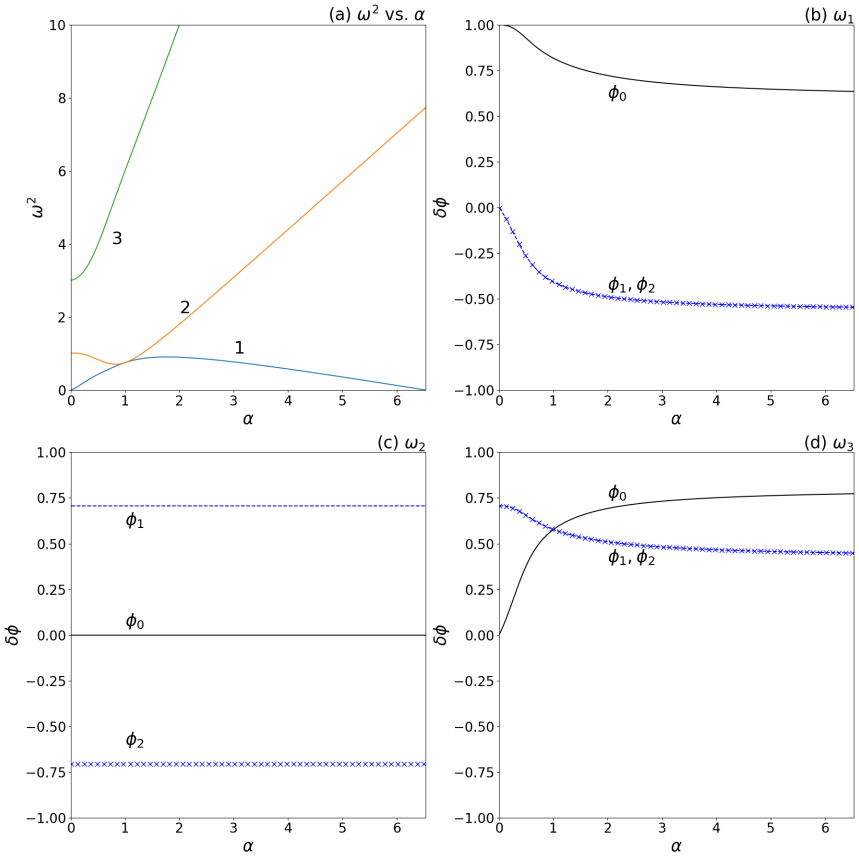

Figure 4.2: The normal mode information for the low α state. The eigenfrequencies in term of the characteristic frequency are illustrated in panel (a). In panels (b) through (d) the solid black curve denotes the displacement from equilibrium of ϕ_0, the dashed and

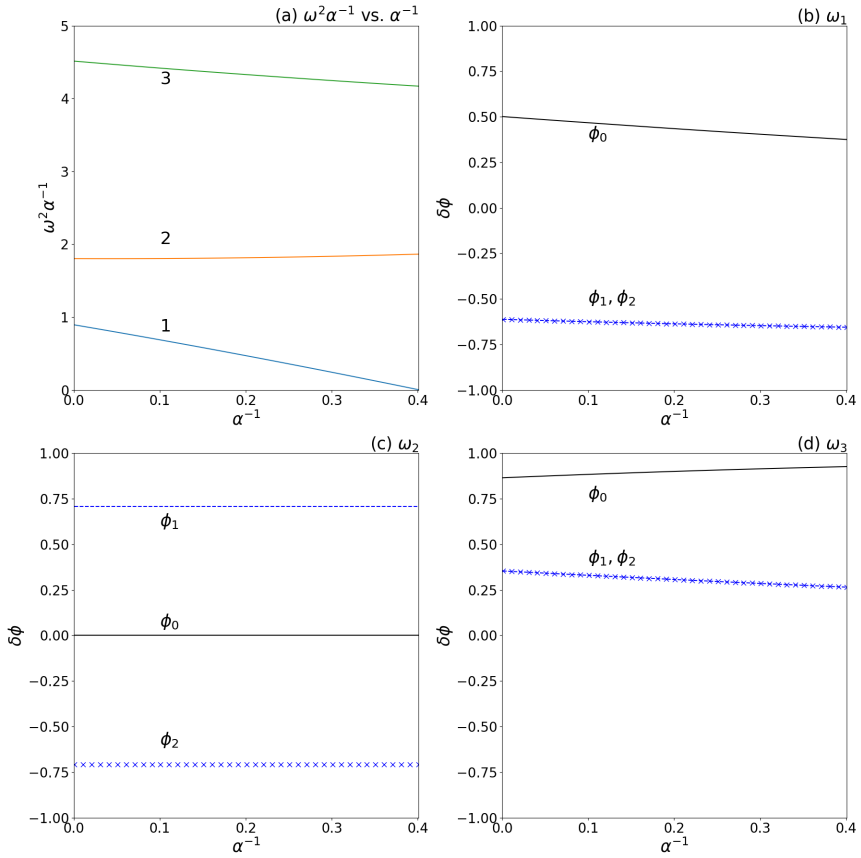

Figure 4.3: The normal mode information for the high α state. The curves are formatted with the same structure as 4.2.

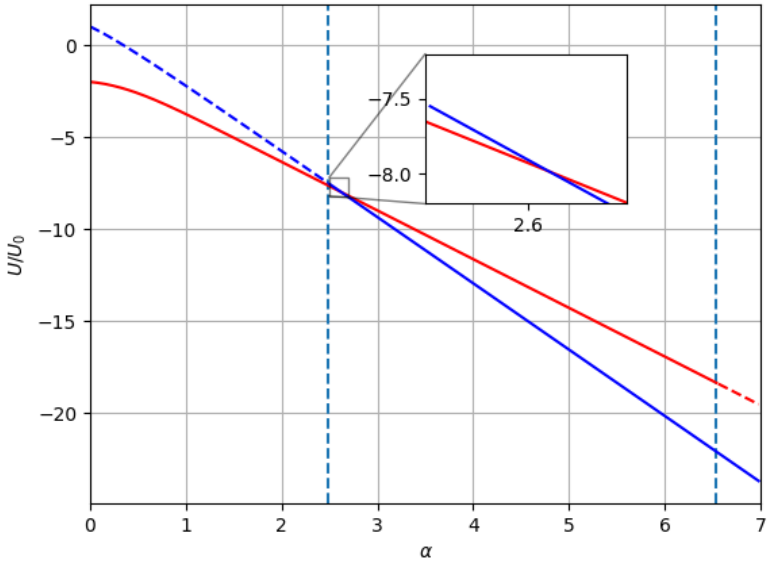

Figure 4.4: These are curves of the potential energy of the ground state as a function of α. Both low and high α states presented. Low α is in red with high α in blue. The dashed portions indicate the regions where they are unstable. The vertical dashed lines represent the critical values where the transitions are forced.

CHAPTER 5

Conclusions

In chapter 2 we examined a system that was a strict superset of a chaotic system. We then showed that counter intuitively the more complicated system exhibited the simpler quasi-periodic motion. However this is only the first of many questions this system raises for future discussion. Using Eq. (2.9) we can explore whether splitting the Hamiltonian works for any set of spheres or if there are certain ratios that must hold. We can also explore stability of circular orbits that likely exist. With the appropriate numerical techniques we can examine how these spheres interact with bouncing. These questions and more are open for investigation.

In chapter 3, a system of seven magnets presents an opportunity to examine bifurcations in a manner that is physically realizable and has few degrees of freedom. The two associated states have qualitatively different normal modes of oscillation and limits. Additionally, the system exhibits hysteresis, transitioning back to the circular state at α_1 which is lower than when it transitions to the dipolar state. As a theoretical system, it suggests additional avenues for investigation. How does the system behave for larger collections of magnets? Insights into the behavior of large collections of dipoles in this configuration may be of application for modeling cylindrical wave guides made of materials with significant molecular dipole moments.

What is the simplest configuration of dipoles that can exhibit hysteresis of this nature? This question is addressed in chapter 4 and was found that a system with as few as three dipoles at the vertices of an equilateral triangle has two overlapping states. An interesting parallel is that three magnets in a one dimensional configuration doesn't even bifurcations. Is there some underlying similarity between this small collection of dipoles and the Ising Model where only in two dimensions or higher can phase changes take place?

REFERENCES

[1] S. Borgers, S. Völkel, W. Schöpf, and I. Rehberg, "Exploring cogging free magnetic gears," *American Journal of Physics*, vol. 86, no. 6, pp. 460–469, 2018. [Online]. Available: https://doi.org/10.1119/1.5029823

[2] G. L. Pollack and D. R. Stump, "Two magnets oscillating in each other's fields," *Canadian Journal of Physics*, vol. 75, no. 5, pp. 313–324, 1997. [Online]. Available: https://doi.org/10.1139/p96-151

[3] D. R. Stump, G. L. Pollack, and J. Borysowicz, "Magnets at the corners of polygons," *American Journal of Physics*, vol. 65, no. 9, pp. 892–897, 1997. [Online]. Available: www.scopus.com

[4] B. F. Edwards, D. M. Riffe, J. . Ji, and W. A. Booth, "Interactions between uniformly magnetized spheres," *American Journal of Physics*, vol. 85, no. 2, pp. 130–134, 2017. [Online]. Available: www.scopus.com

[5] B. F. Edwards and J. M. Edwards, "Periodic nonlinear sliding modes for two uniformly magnetized spheres," *Chaos*, vol. 27, no. 5, 2017. [Online]. Available: www.scopus.com

[6] B. F. Edwards, B. A. Johnson, and J. M. Edwards, "Periodic bouncing modes for two uniformly magnetized spheres. i. trajectories," *Chaos: An Interdisciplinary Journal of Nonlinear Science*, vol. 30, no. 1, p. 013146, 2020. [Online]. Available: https://doi.org/10.1063/1.5125924

[7] B. F. Edwards, B. A. Johnson, and J. M. Edwards, "Periodic bouncing modes for two uniformly magnetized spheres. ii. scaling," *Chaos: An Interdisciplinary Journal of Nonlinear Science*, vol. 30, no. 1, p. 013131, 2020. [Online]. Available: https://doi.org/10.1063/1.5125925

[8] T. H. Boyer, "The force on a magnetic dipole," *Am.J.Phys.*, vol. 56, no. 8, pp. 688–692, 1988, cited By :94. [Online]. Available: www.scopus.com

[9] L. Vaidman, "Torque and force on a magnetic dipole," *Am.J.Phys.*, vol. 58, no. 10, pp. 978–983, 1990, cited By :100. [Online]. Available: www.scopus.com

[10] D. J. Griffiths, "Dipoles at rest," *Am.J.Phys.*, vol. 60, pp. 979–987, 1992, cited By :34. [Online]. Available: www.scopus.com

[11] V. Hnizdo, "Hidden mechanical momentum and the field momentum in stationary electromagnetic and gravitational systems," *American Journal of Physics*, vol. 65, no. 6, pp. 515–518, 1997, cited By :12. [Online]. Available: www.scopus.com

[12] D. J. Griffiths, *Introduction to Electrodynamics*, 1989. [Online]. Available: www.scopus.com

[13] E. P. Furlani, R. Wang, and H. Kusnadi, "A three-dimensional model for computing the torque of radial couplings," *IEEE Transactions on Magnetics*, vol. 31, no. 5, pp. 2522–2526, 1995. [Online]. Available: www.scopus.com

[14] J. R. Taylor, *Classical Mechanics*. University Science Books, 2005.

[15] J. Schönke, "Smooth teeth: Why multipoles are perfect gears," *Phys. Rev. Applied*, vol. 4, p. 064007, Dec 2015. [Online]. Available: https://link.aps.org/doi/10.1103/PhysRevApplied.4.064007

[16] D. R. Stump and G. L. Pollack, "Magnetic dipole oscillations and radiation damping," *American Journal of Physics*, vol. 65, no. 1, pp. 81–87, 1997. [Online]. Available: www.scopus.com

[17] F. M. S. Lima, "Analytical study of the critical behavior of the nonlinear pendulum," *American Journal of Physics*, vol. 78, no. 11, pp. 1146–1151, 2010. [Online]. Available: https://doi.org/10.1119/1.3442472

[18] A. Smith, P. T. Haugen, and B. F. Edwards, "Phase transitions and hysteresis for seven rotating magnetic dipoles: Equilibria," *in review*. [Online]. Available: www.scopus.com

[19] P. T. Haugen and B. F. Edwards, "Dynamics of two freely rotating dipoles," *American Journal of Physics*, vol. 88, no. 5, pp. 365–370, 2020. [Online]. Available: https://doi.org/10.1119/10.0000625

[20] E. Fehlberg, *Low-order Classical Runge-Kutta Formulas with Stepsize Control and Their Application to Some Heat Transfer Problems*, ser. NASA technical report. National Aeronautics and Space Administration, 1969. [Online]. Available: https://books.google.com/books?id=IMaJw5g4hGkC

[21] C. R. Harris, K. J. Millman, S. J. van der Walt, R. Gommers, P. Virtanen, D. Cournapeau, E. Wieser, J. Taylor, S. Berg, N. J. Smith, R. Kern, M. Picus, S. Hoyer, M. H. van Kerkwijk, M. Brett, A. Haldane, J. F. del R'ıo, M. Wiebe, P. Peterson, P. G'erard-Marchant, K. Sheppard, T. Reddy, W. Weckesser, H. Abbasi, C. Gohlke, and T. E. Oliphant, "Array programming with NumPy," *Nature*, vol. 585, no. 7825, pp. 357–362, Sep. 2020. [Online]. Available: https://doi.org/10.1038/s41586-020-2649-2

[22] C. Shannon, "Speech at bell labs on creative thinking," Mar. 1952.

Peter Haugen

Utah State University

Department of Physics

Science and Engineering Research

Logan, UT, 84321

Phone: (319) 325-7978

Email: phaugen@gmail.com

github: https://github.com/wolfram74

Personal

Born on October 9, 1988.

United States Citizen.

Education

High School Diploma, Iowa City West High School, 2007.

B.S. Physics, University of Iowa, 2012.

Minor in Chemistry, University of Iowa, 2012

Introduction to Algorithms part 1, Stanford, 2013

Visiting Research Scholar, University of California Berkeley Physics Department, 2013-2014

Developer Bootcamp Web Programming intensive, 2015

Machine Learning, Stanford, 2015

Utah State University, Doctorate in Physics, 2017-present

Employment

University of Iowa Physics Department Student Labs 2007.

University of Iowa Secondary Student Training Program 2008–2010.

Developer Bootcamp Teaching Assistant 2015.

Coderpad Inc 2015-2016.

Developer Bootcamp Remote Instructor 2016-2017

Research Experiences

Labs

Dr. Johna Leddy: Electrochemistry 2006-2007

Dr. Ed Gillan: Inorganic Synthesis 2008

Dr. Alexi Tivanski: Atomic Force Microscopy 2009

Dr. Fred Skiff: Fundamental Plasma Physics 2010-2012

Dr. Joel Fajans: Non-Neutral Plasma Confinement 2014

Dr. Boyd Edwards: Nonlinear and Chaotic Mechanics 2017-2022

Publications

Dynamics of two freely rotating dipoles

Hysteretic transition between states of a filled hexagonal magnetic dipole cluster

Normal-mode oscillations for the circular and dipolar states of a filled hexagonal magnetic dipole cluster

Community Contributions

Coordinator for We Can Code Workshop supported by USU Physics Department, 2017-present

Director of and lead instructor for We Can Code Workshop supported by Iowa City Public Library, 2016-2017

Assisting Dale Stille in outreach events for the University of Iowa's Physics department, 2009-2012

LEAD tutoring with Neighborhood Centers of Johnson County 2012

Treasurer for University of Iowa chapter of Student Physics Society 2011-2012